cluded in the KUR beam is effective for enlarging the thermal neutron flux at parts deep within the body. This is because the RB-BNCT system can maximize the dose sent to deep-seated tumors near 10 cm, as well as the AB-BNCT system (Figs. 3B and 4B).

Some authors have already reported the advantage of AB-BNCT for deep-seated brain tumors over RB- BNCT using a head phantom. Burlon et al. have reported that AB-BNCT can treat brain tumors that are ~2.0 cm deeper than those treated with RB-BNCT [19]. Blue et al. have reported that, for treatment of brain tumors, compared with RB-BNCT, AB-BNCT can create a neutron field with a significantly better field quality (by a factor of 1.2), which is judged by the dose that can be delivered to a tumor at a depth of 6 cm [20]. The present study is believed to be the first to describe the advantages of AB-BNCT over RB-BNCT in the treatment of body trunk tumors, multiple liver tumors and MPM, apart from brain tumors.

We are preparing to undertake clinical trials with our AB-BNCT system to get an approval as a medical device from the Pharmaceuticals and Medical Devices Agency (PMDA), a Japanese regulatory agency. This approval is a prerequisite before the AB-BNCT system can be constructed at medical institutes. As revealed in the present study, AB-BNCT has the potential to be applied to multiple liver tumors and MPM. The patients with multiple liver tumors, including metastatic tumors or hepatocellular carcinomas, are much greater in number than malignant gliomas or melanomas, which have been treated with BNCT in Japan, the United States and Europe. Selective high-LET irradiation to tumor cells by BNCT has the potential to shed new light on the best way to treat multiple metastatic tumors in lung or brain and pleuritis carcinomatosis. Extending the application of BNCT to many malignancies will lead to further progress in the field of BNCT. After approval of the AB-BNCT system as a medical device, it will be on the market and installed in existing hospitals.

In conclusion, the AB-BNCT system constructed at our institute has the ability to deliver three- or four-port irradiation in the treatment of multiple liver tumors and MPM within a reasonable treatment time (30–60 min). In addition, the AB-BNCT system has advantages over RB-BNCT for the treatment of deep-seated tumors. AB-BNCT has the potential to be a promising treatment option for patients with multiple liver tumors and MPM.

References

[1] Coderre JA, Morris GM. The radiation biology of boron neutron capture therapy. Radiat Res 1999;151:1–18.

[2] Barth RF, Joensuu H. Boron neutron capture therapy for the treatment of glioblastomas and extracranial tumours: as effective, more effective or less effective than photon irradiation? Radiother Oncol 2007;82:119–22.

[3] Suzuki M, Masunaga S, Kinashi Y, et al. Intra-arterial administration of sodium borocaptate (BSH)/lipiodol emulsion delivers B-10 to liver tumors highly selectively for boron neutron capture therapy: experimental studies in the rat liver model. Int J Radiat Oncol Biol Phys 2004;59:260–6.

[4] Suzuki M, Sakurai Y, Masunaga S, et al. Preliminary experimental study of boron neutron capture therapy for malignant tumors spreading in thoracic cavity. Jpn J Clin Oncol 2007;37:245–9.

[5] Suzuki M, Sakurai Y, Masunaga S, Kinashi Y, Nagata K, Ono K. Dosimetric study of boron neutron capture therapy with borocaptate sodium (BSH)/lipiodol emulsion (BSH/lipiodol-BNCT) for treatment of multiple liver tumors. Int J Radiat Oncol Biol Phys 2004;58:892–6.

[6] Suzuki M, Sakurai Y, Masunaga S, et al. Feasibility of boron neutron capture therapy (BNCT) for malignant pleural mesothelioma from a viewpoint of dose distribution analysis. Int J Radiat Oncol Biol Phys 2006;66:1584–9.

[7] Suzuki M, Sakurai Y, Hagiwara S, et al. First attempt of boron neutron capture therapy (BNCT) for hepatocellular carcinoma. Jpn J Clin Oncol 2007;37:376–81.

[8] Suzuki M, Endo K, Satoh H, et al. A novel concept of treatment of diffuse or multiple pleural tumors by boron neutron capture therapy (BNCT). Radiother Oncol 2008;88:192–5.

[9] Lee CL, Zhou XL, Kudchadker RJ, Harmon F, Harker YD. A Monte Carlo dosimetry-based evaluation of the ^{7}Li(p,n)^{7}Be reaction near threshold for accelerator boron neutron capture therapy. Med Phys 2000;27:192–202.

[10] Tanaka H, Sakurai Y, Suzuki M, et al. An epithermal neutron generator based on the Be(p,n) reaction using a 30 MeV proton cyclotron accelerator at KURRI. In: Zonta A, Altieri S, Roveda L, Barth R, editors. 13th International Congress on Neutron Capture Therapy "A new option against cancer". Roma: ENEA; 2008. p. 510–3.

[11] IAEA. Current status of neutron capture therapy. In: IAEA TECDOC 1223, Vienna: IAEA; 2001. p. 6–8.

[12] Sakurai Y, Kobayashi T. Controllability of depth dose distribution for neutron capture therapy at the heavy water neutron irradiation facility of Kyoto University Research Reactor. Med Phys 2002;29:2338–50.

[13] Sakurai Y, Kobayashi T. The medical-irradiation characteristics for neutron capture therapy at the heavy water neutron irradiation facility of Kyoto University Research Reactor. Med Phys 2002;29:2328–37.

[14] Kawabata S, Miyatake S, Kajimoto Y, et al. The early successful treatment of glioblastoma patients with modified boron neutron capture therapy. Report of two cases. J Neurooncol 2003;65:159–65.

[15] Kato I, Ono K, Sakurai Y, et al. Effectiveness of BNCT for recurrent head and neck malignancies. Appl Radiat Isot 2004;61:1069–73.

[16] Suzuki M, Masunaga S, Kinashi Y, et al. The effects of boron neutron capture therapy on liver tumors and normal hepatocytes in mice. Jpn J Cancer Res 2000;91:1058–64.

[17] Kiger JL, Kiger WS, Patel H, et al. Functional and histological assessment of the radiobiology of normal rat lung in BNCT. In: Nakagawa Y, Kobayashi T, Fukuda H, editors. Advances in neutron capture therapy 2006. Takamatsu: ISNCT; 2006. p. 85–8.

[18] Ono K, Nagata Y, Akuta K, Abe M, Ando K, Koike S. Frequency of micronuclei in hepatocytes following X and fast-neutron irradiations-an analysis by a linear-quadratic model. Radiat Res 1990;123:345–7.

[19] Burlon AA, Kreiner AJ. A comparison between a TESQ accelerator and a reactor as a neutron sources for BNCT. Nucl Instr Meth Phys Res B 2008;266:763–71.

[20] Blue TE, Yanch JC. Accelerator-based epithermal neutron sources for boron neutron capture therapy of brain tumors. J Neurooncol 2003;62:19–31.
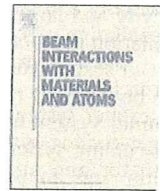
Characteristics comparison between a cyclotron-based neutron source and KUR-HWNIF for boron neutron capture therapy

H. Tanaka [a,*], Y. Sakurai [a], M. Suzuki [a], S. Masunaga [a], Y. Kinashi [a], G. Kashino [a], Y. Liu [a], T. Mitsumoto [b], S. Yajima [b], H. Tsutsui [b], A. Maruhashi [a], K. Ono [a]

[a] Research Reactor Institute, Kyoto University, Asashiro-nishi 2-1010, Kumatori-cho, Osaka 590-0494, Japan
[b] Sumitomo Heavy Industries, Osaki 2-1-1, Shinagawa, Tokyo 141-6025, Japan

ARTICLE INFO

ABSTRACT

At Kyoto University Research Reactor Institute (KURRI), 275 clinical trials of boron neutron capture therapy (BNCT) have been performed as of March 2006, and the effectiveness of BNCT has been revealed. In order to further develop BNCT, it is desirable to supply accelerator-based epithermal-neutron sources that can be installed near the hospital. We proposed the method of filtering and moderating fast neutrons, which are emitted from the reaction between a beryllium target and 30-MeV protons accelerated by a cyclotron accelerator, using an optimum moderator system composed of iron, lead, aluminum and calcium fluoride. At present, an epithermal-neutron source is under construction from June 2008. This system consists of a cyclotron accelerator, beam transport system, neutron-yielding target, filter, moderator and irradiation bed.

In this article, an overview of this system and the properties of the treatment neutron beam optimized by the MCNPX Monte Carlo neutron transport code are presented. The distribution of biological effect weighted dose in a head phantom compared with that of Kyoto University Research Reactor (KUR) is shown. It is confirmed that for the accelerator, the biological effect weighted dose for a deeply situated tumor in the phantom is 18% larger than that for KUR, when the limit dose of the normal brain is 10 Gy-eq. The therapeutic time of the cyclotron-based neutron sources are nearly one-quarter of that of KUR. The cyclotron-based epithermal-neutron source is a promising alternative to reactor-based neutron sources for treatments by BNCT.

© 2009 Elsevier B.V. All rights reserved.

1. Introduction

Boron neutron capture therapy (BNCT) is a modality to kill a cancer cell by an α particle and a Li nucleus emitted from the capture reaction between a thermal neutron and a ^{10}B atom added in the medicine that easily accumulates in a cancer cell. The emitted α particle and Li nucleus have short ranges of 9 μm and 5 μm, respectively, and total range is 14 μm corresponding to the cell size. As a result, their energy is mostly deposited within a cell. Therefore, BNCT is a unique modality that has higher cell selectivity than other radiotherapies.

At first, the BNCT treatments using Kyoto University Research Reactor (KUR) were adapted for malignant melanoma and brain tumors. Heavy-water neutron irradiation facility (HWNIF) of KUR was upgraded in March 1996. Its wide application to the treatment of the other disease such as recurrent head and neck tumors, liver tumors [1], and mesothelioma [2] using epithermal-neutrons has

resulted in an increase in the number of trial cases. Seventy percent of the cases were treated after December 2001. In order to obtain good treatment results for a deeply situated body tumor, a higher dose is required.

KUR has been stopping the operation since March 2006 because of the return of high-enriched uranium fuels. However, we have a plan to install low-enriched uranium fuels to operate KUR for one decade. More clinical trials will be carried out to show the effectiveness of BNCT. Moreover, a sufficient neutron yield obtained by using an accelerator-based neutron source that can be located near a hospital is required for the further development of BNCT.

Some groups are already investigating a neutron source using spallation reactions between several tens of MeV protons and heavy materials such as lead, tungsten and tantalum [3,4]. As for the combination of several tens of MeV protons and a beryllium target, the examination was excluded because of the contamination of the treatment beam (epithermal-neutron beam) by fast neutrons. However, we confirmed that a sufficient epithermal-neutron yield based on the Be(p,n) reaction could be obtained with an optimum beam-shaping assembly. Our system has the advantage of lower

* Corresponding author. Tel.: +81 72 451 2468; fax: +81 72 451 2620.
E-mail address: h-tanaka@rri.kyoto-u.ac.jp (H. Tanaka).

activity and larger neutron yield of targets as compared with the spallation reactions involving heavy materials.

Our system consists of a cyclotron accelerator promising a proton beam of ~1 mA at 30 MeV, a beam transport system, a beam scanner system for heat reduction on the beryllium target, a target-cooling system, a beam-shaping assembly, a multi-leaf collimator and an irradiation bed for patients in both sitting and decubitus positions. We simulated the neutronics for optimum treatment beams using the Monte Carlo calculation code MCNPX [5]. In this article, we report the system of our epithermal-neutron generator and the simulated characteristics compared with that of KUR.

2. Materials and methods

2.1. Cyclotron-based neutron source (CBNS)

2.1.1. Accelerator and beam transport

Fig. 1 shows schematic layout of a cyclotron-based neutron source in Innovation Research Laboratory Medical Area at KURRI. We employ the cyclotron accelerator (HM-30) manufactured by Sumitomo Heavy Industries (SHI) to promise ~1 mA at 30 MeV proton beam. SHI has the technology to manufacture various types of cyclotron accelerators for the production of radioactive medicines for positron emission tomography (PET). Accelerating particles of HM-30 are hydrogen negative ions, and the particles accelerated up to 30 MeV are derived by the charge conversion in a carbon foil stripper. HM-30 dimensions of 3030-mm width × 1620-mm length × 1724-mm height. A proton beam derived from HM-30 is led to the beryllium target via a beam transport system. Two electromagnetic scanning coils are inserted at the end of the beam transport system for beam spread in order to reduce the heat produced in the Be target. A uniform proton beam with a square shape of 120 mm × 120 mm is formed by controlling magnetic field of each scanning magnet. The principle of scanning

Fig. 1. Schematic layout of cyclotron-based neutron source.

is to use the difference of the scanning frequencies between the X- and Y-axes magnets excited by triangle waves.

2.1.2. Beryllium target

In order to select a suitable target material, it is important to consider the characteristics such as neutron yield, neutron energy, thermal properties and the activation on proton irradiation in terms of the maintenance of a target. Table 1 shows the characteristics of Li, Be, W and Ta as target materials when irradiated by a 1-mA, 30-MeV proton beam. The neutron and gamma-ray yields were estimated by MCNPX and the cross-section data. The target thickness is more than the range of protons at 30 MeV in each of the target materials. In order to calculate the neutron yield of the Ta target, the LAHET code [6] with a physics model was used because the evaluated nuclear-cross-section data of La150 do not contain Ta data.

Among the materials listed in Table 1, Be has the highest neutron yield and the smallest gamma-ray yield per neutron. The neutron yield is high in the order of Ta, W and Li. Because of the low melting point of Li, it is difficult to maintain a Li target stable under 1-mA, 30-MeV proton beam irradiation.

Further, in Table 1, Be has the highest thermal conductivity and a high melting point. A 1-mA, 30-MeV proton beam has a power of 30 kW; this implies a heat input of 30 kW to the target irradiated using this beam. Such a large heat input necessitates a target-cooling system. In our system, a Be target is directly cooled by pure compressed water. The compressed water flows through a spiral graphite water channel; the graphite is prevented from activation. Protons (30-MeV) with a range of 5.8 mm in Be penetrate a 5.5-mm-thick Be target and inject in the compressed cooling water in order to prevent blistering of the target. Most of the low-energy protons with an energy of less than 2 MeV cannot produce neutrons while passing through Be because the threshold energy of reaction between proton and Be is ~2 MeV.

With regard to the experimental results for the thermal resistance of a Be target, Tadokoro et al. indicated that a heat input of 500 W/cm^2 leads to a temperature of less than 500 °C [7]. The irradiation area should be expanded to 144 cm^2 for a heat input of 200 W/cm^2 under 30-kW operation.

The activation of a target should be as low as possible in order to avoid additional expenses that are otherwise incurred by remote handling devices and heavy radiation shielding. Low activation is also important for hospital management with regard to the maintenance, storage and control of targets.

For evaluating target activation resulting from one year of operation we assumed 2-h irradiation per day with a proton current of 1 mA. Fig. 2 shows the relationship between the ambient dose equivalent at 1 cm and the elapsed time after one year of operation. Induced radioactivity analysis code (IRAC) can calculate the neutron- and proton-induced activation of target material [8]. The nuclei produced in a W target have higher activity and longer half lives than Be and Ta targets. Immediately after one year of operation, the activation rate of a Ta target is four order of magnitude higher than that of a Be target. The period required by the Ta target until the ambient dose rate becomes 1 mSv/h, is twice of that required by the Be target. Considering the above-mentioned results in terms of the neutron yield, thermal properties, and activation level, we selected the Be target.

2.1.3. Beam-shaping assembly

Yanch et al. revealed that for BNCT treatments at a 10-cm depth of the head, 10 keV is the most effective neutron energy and 4 eV to 40 keV is the most effective energy range [9]. In terms of the design of an accelerator-based moderator, it is necessary to form the neutron irradiation field with an energy spectrum peaking at around 10 keV. In the reaction between 30-MeV protons and a Be target,
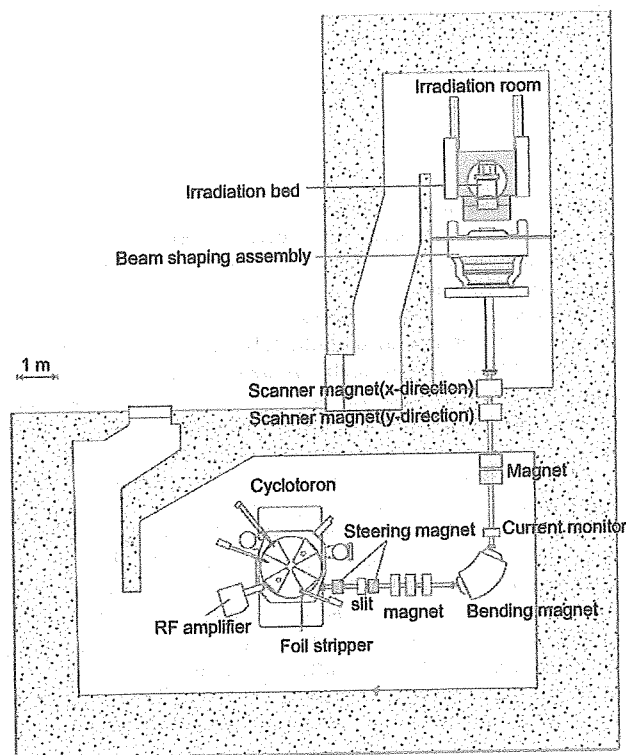
Table 1
Target material property compared with Li, Be, Ta and W.

Target	Melting point (°C)	Boiling point (°C)	Thermal conductivity (W/m/K)	Neutron yield (/s/mA)	Gamma-ray yield (s/mA)	Gamma-ray yield per one neutron	Cross-section data
Li	180	1340	84.7	1.14E+14	9.80E+12	0.09	ENDF-VII
Be	1278	2970	201	1.90E+14	3.35E+12	0.02	ENDF-VII
Ta	3017	5458	57.5	1.27E+14	1.18E+14	0.93	Physics model
W	3422	5555	174	9.65E+13	1.35E+14	1.40	la150

the neutrons that are emitted forward direction have an energy of up to 28 MeV. Therefore, in order to treat a deep tumor, it is necessary to reduce the neutron energy to the range of epithermal energy. For this purpose, our system has two components: a moderator and a shaper. The moderator is used to reduce the energy from the maximum value of 28 MeV with low capture cross-section. The shaper is used to obtain the optimum energy such as 10 keV mentioned above.

Fig. 3 shows the schematic layout of the moderator, shaper, (called beam-shaping assembly: BSA) and irradiation room. The moderator materials are Pb and Fe. Pb has a cross-section of ~1 barn for the (n,2n) reaction with the maximum neutron energy of larger than 10 MeV. Further, Pb has the inelastic scattering cross-section of ~1 barn for the incident neutron energy of larger than 1 MeV. Fe has a smaller cross-section for the (n,2n) reaction than Pb has, but the inelastic scattering cross-section of Fe is larger than that of Pb at an incident neutron energy of several MeV. Therefore, a Pb component was installed near the target region and a Fe component was installed after the Pb component. The Pb component was placed around the Be target assembly as a reflector in order to reflect the neutrons that were back-scattered by the Be target. The target assembly is removable in order to facilitate target replacement.

The shaper is made of Al and CaF_2 and serves to reduce the neutron energy to the epithermal energy region. The total neutron cross-section of Al exhibits valleys at incident neutron energies of around 27 and 70 keV. This implies that the neutrons with these energies have a small probability of reacting with Al. Further, although 70-keV neutrons raise the normal dose, F has the resonance cross-section at a neutron energy of larger than several tens keV. Consequently, the combination of Al and F limits the neutron energy to around 27 keV.

The combination of 69% AlF_3, 30% Al and 1% ^6LiF (called FLUEN-TAL^n developed by VTT Corporation at Finland) is often used in the design of an epithermal-neutron generator [10]. In order to obtain
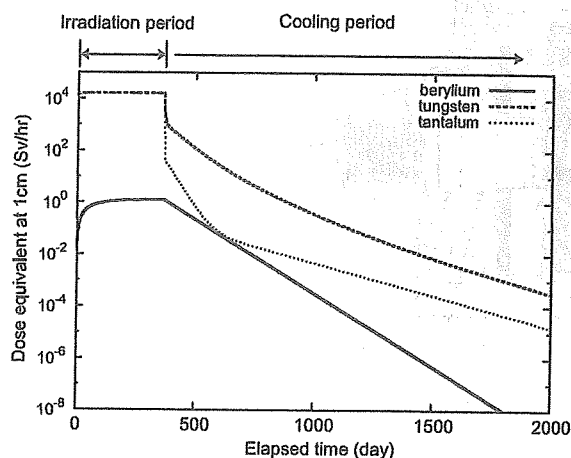
intense neutron flux, the moderator and shaper size should be small with sufficient ability for moderating and shaping. It is recommended that the material density of the shaper should be high.

FLUENTAL^n is supplied as powder; it is difficult to increase its density because AlF_3 sublimes at a temperature of 1040 °C under atmospheric pressure. Therefore, we focus our attention on CaF_2 that is easily available on a commercial basis. CaF_2 dose not have good mechanical strength; therefore, it was formed in a disk shape and placed in an Al container.

Epithermal neutrons are passed through the moderator and shaper and led to a collimator that is placed after a gamma shield made of Pb. The collimator is composed of ^{nat}LiF-loaded polyethylene blocks having a thickness of 1.5 cm. The collimator aperture can be adjusted up to $\phi25$ cm and formed to any shape in order to fit the irradiation field. Patients can easily seat to insert the foot in the cone shape of the collimator.

Fig. 4 shows the calculation results of energy reduction process in the moderator and shaper. After the neutrons have passed through the moderator, which is composed of Pb and Fe, their energy spectrum exhibits a peak at 1 MeV. This implies that the moderator can effectively reduce the energy that is higher than 1 MeV. After coming out of the moderator, these neutrons pass through the shaper, which is composed of Al and CaF_2, that further reduces their energy from 1 MeV to the epithermal-neutron region of 10–20 keV. The optimum thickness of each component was determined by the Monte Carlo simulation using the property of the distribution of biological effect weighted dose in a phantom.

In order to prevent the exposure of a patient to fast-neutron radiation, the moderator and shaper (particularly the front surface of the collimator) are surrounded by polyethylene blocks. These polyethylene blocks also serve as a shield around the irradiation room.

Fig. 2. Relationship between the elapsed time after one-year irradiation operation and the activation of Be, W and Ta targets.
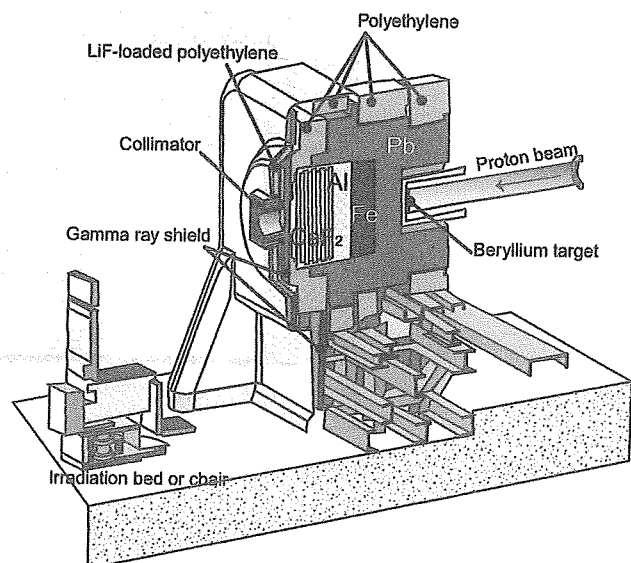

Fig. 3. Schematic layout of a beam-shaping assembly for epithermal neutron generator using 30-MeV proton cyclotron and Be target.
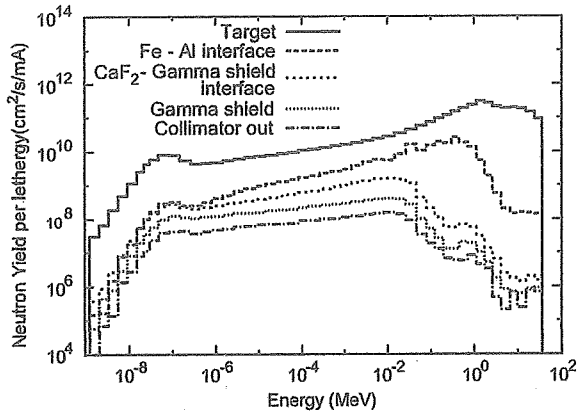
Fig. 4. Neutron energy spectrum at each evaluation point of a beam-shaping assembly.

Fig. 6. Comparison with neutron spectrum at a gamma shield for KUR and CBNS.

In order to help the patient to take a comfortable irradiation position, an irradiation bed can be moved from right to left, or up and down, or back and forth. The irradiation bed and collimator can also be moved back; before switching on the treatment irradiation, the irradiation area can be confirmed by a view taken from the beam direction through the collimator aperture.

Further, so as to accurately set the patient in the position determined by the treatment planning system, an X-ray tube and an imaging plate are installed. The irradiation position is determined by comparing a bone image obtained by treatment planning (reconstructed by CT images) and the X-ray image of the imaging plate. The pair of X-ray tube and imaging plate can be moved to the neutron beam side and an image of the "beam's eye view" can be obtained. Laser markers are also installed; the irradiation position was set by the marking on the skin.

2.2. Reactor-based neutron source

2.2.1. Kyoto University Reactor (KUR)

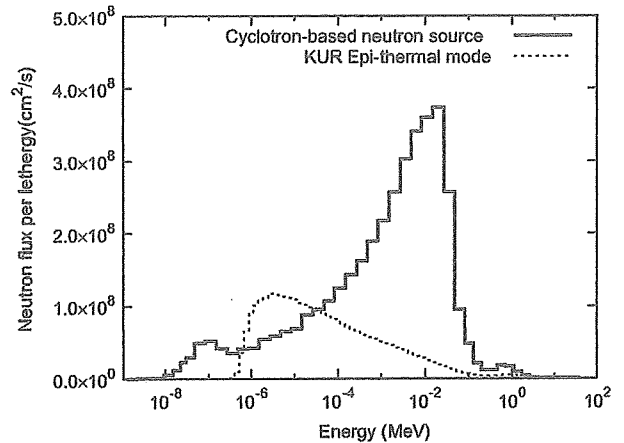KUR is a light-water-moderated, tank-type nuclear research reactor with a nominal power of 5 MW. It has been widely utilized for several research fields in various subject areas such as physics, chemistry, biology, engineering, agriculture, medicine, etc. since the first criticality in June 1964.

2.2.2. Heavy-water neutron irradiation facility (HWNIF)

HWNIF is a medical facility installed in KUR. The details of this facility are described in reference [11]. Fig. 5 shows schematic layout of HWNIF. The high-energy neutrons produced by fission reactions in core are moderated by the epithermal-neutron moderator, which is a mixture of aluminum and heavy-water ($Al:D_2O =$ 80%:20% in volume). A heavy-water spectrum shifter is installed outside of the epithermal-neutron moderator. The total heavy-water thickness can be changed from 0 to 90 cm in 10-cm increments for changing to various neutron spectrums. Thermal-neutron filters made of cadmium and boral are installed outside of the spectrum shifter, for the regulation of the thermal-neutron component and the formation of epithermal neutrons. Outside of these filters, a bismuth layer is placed for gamma-ray elimination. In this facility, neutron beams with various energy spectra from almost pure thermal to epithermal are obtained by controlling the
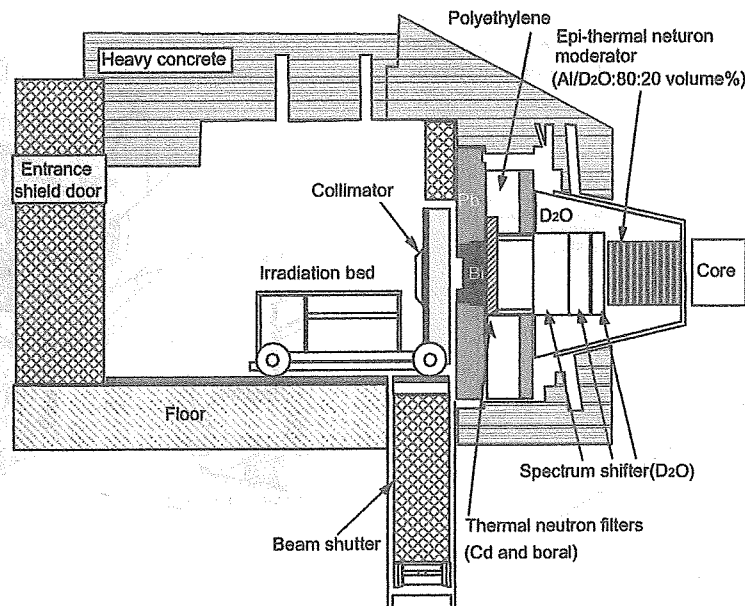

Fig. 5. Schematic layout of HWNIF at KUR.

Table 2
Beam property of CBNS under free-air condition compared with KUR epithermal mode.

	Epi-thermal neutron flux (Φ_{epi}) (n/cm^2/s)	Fast-neutron dose/Φ_{epi} (Gy/n cm^2)	Gamma-ray dose/ Φ_{epi} (Gy/n cm^2)
KUR (epi-thermal)	7.30E+08	9.10E−13	2.40E−13
Accelerator	1.88E+09	5.84E−13	7.75E−14

heavy-water thickness in the spectrum shifter and by opening and closing of the cadmium and boral thermal neutron filters. BNCT using epithermal-neutron irradiation was started in earnest in December 2001 at HWNIF. As of March 2006, 189 BNCT treatments using epithermal-neutron incidence were carried out: 82 for brain tumors, 93 for recurrent head and neck tumors, and 14 for body tumors.

2.3. Beam properties

Fig. 6 shows the neutron spectrum evaluated at the surface of gamma-ray shielding. In this calculation, the collimator was removed because of the free-air condition. The spectrum of KUR is also plotted in Fig. 6. This epithermal-neutron spectrum formed by using a cadmium thermal neutron filter of KUR is most-often used in BNCT treatment.

The accelerator-based neutron spectrum has a peak in the energy range of 10–20 keV. In the case of this spectrum, the definition of the energy range of epithermal is from 0.5 eV to 40 keV, because as mentioned above (Section 2.1.3), this region is most effective for the treatment of deep tumors. In this article, the energy region below 0.5 eV is defined as the thermal region; that above 40 keV, as the fast-neutron region. In comparison with KUR, CBNS has the potential of better treatment effectiveness because of a better energy spectrum.

Table 2 shows the contamination of absorbed dose by fast-neutron and gamma-ray components under the free-air condition. Each absorbed dose was derived from the neutron flux at the position of the gamma-ray shield and the conversion factor to the absorbed dose published in ICRP-74 [12]. The human component was assumed to be H: 11.1, C: 12.6, N: 2.0 and O: 74.3 (wt%). It is confirmed that with regard to the contaminations caused by fast neutrons and gamma rays, CBNS is superior to KUR. The epithermal-neutron flux of CBNS was larger than that of KUR by a factor of 2.5.

In order to confirm the beam flatness, the neutron flux was evaluated at the collimator surface with the collimator aperture
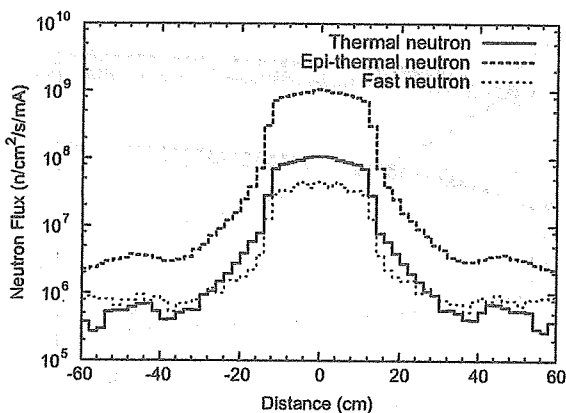

Fig. 7. Flux distribution of thermal, epithermal and fast neutrons as a function of distance from beam axis.

of ϕ25 cm. Fig. 7 shows the relationship between flux distribution of thermal-, epithermal- and fast-neutrons and the distance from beam axis. As compared with its value at the beam axis, the epithermal-neutron flux at a distance of 5 cm from the beam axis and at the collimator edge reduced by 10% and 30%, respectively. Because neutrons pass through a material with some scattering reaction with it, reducing their energy, the treatment beam contained neutrons having several directions. However, in actual treatment, the patient is positioned directly in front of the collimator and neutrons that are injected into the patient's body diffuse. Therefore, to use our treatment beam compared with completely flat beam has a little influence in treatment effectiveness.

The thermal-, epithermal- and fast-neutron flux decreased at locations far from the beam axis. At a distance of 40 cm from the beam axis, each flux attenuated by two orders of magnitude. It is confirmed that the absorbed dose also reduced at this distance.

3. Results and discussion

3.1. Comparison of beam characteristics in phantom

At KURRI, BNCT clinical trials have been performed using epithermal neutrons. In order to evaluate the dose distribution in a patient's body, the treatment planning system of SERA (Simulation Environment for Radiotherapy Applications) [13,14] was used. For evaluating the properties of CBNS, the experience of past clinical trials using SERA in KUR is referred. In terms of the distribution of thermal-neutron flux in a phantom, it is revealed that the experimental data agree well with the calculated data of SERA within an error of 3% [15].

SERA can make a voxel model for three-dimensional neutron transport calculation using CT/MRI images and output the neutron flux and gamma-ray flux at each voxel. The absorbed dose is derived from the multiplication between the conversion factor served by SERA and the neutron and gamma-ray flux at each voxel.

The main absorbed dose in BNCT consists of the boron dose by the ^{10}B(n,α)^{7}Li reaction, the nitrogen dose by the ^{14}N(n,p)^{14}C, the hydrogen dose by the ^{1}H(n,n')^{1}H, the gamma dose in patient's body by the ^{1}H(n,γ)^{2}H, and the gamma dose produced by the components of BSA and collimator.

The source information for CBNS of SERA, such as neutron and gamma-ray spectrum and angular distribution, is derived from the calculation output of MCNPX. The source information of KUR is epithermal-neutron mode, which is used for actual treatment in KUR. As the parameter for evaluation of epithermal neutron sources, therapeutic time and advantage depth (AD) and advantage depth at 30 Gy-eq (AD30) are used.

AD is the depth in the phantom for a tumor dose distribution of 10 Gy-eq, when the peak of the normal brain dose is 10 Gy-eq. It corresponds to a larger dose that is prescribed for a deep tumor.

We selected the value of 10 Gy-Eq as maximum allowed dose in order to limit the cumulative dose to normal brain tissue lower than 100 Gy. Mayer et al. showed that radiation-induced normal brain tissue necrosis was found to occur at larger than 100 Gy [16]. In our facility, the BNCT treatments were adapted for recurrent brain tumors that were already treated by the conventional radiotherapy up to 60–70 Gy in 2-Gy fractions. To evaluate the cumulative dose to normal brain tissue after BNCT treatment, assuming an α/β coefficient of 3 for normal brain tissue, according to the linear-quadratic model, in single-fractionated BNCT, a 10 Gy-Eq single dose would equal radiation doses of 26 Gy in 2-Gy fractions [17]. Total cumulative dose to normal brain tissue is sufficiently lower than 100 Gy.

On the other hand, Laramore et al. showed a tumor dose-response curve for BNCT. They noted that approximately 30 Gy-Eq

must be given to the tumor [18]. Thus, we defined AD30 for tumor dose. The dose distribution in the phantom is compared between CBNS and KUR. Fig. 8 shows a schematic layout of the irradiation in BNCT for a brain tumor.

In the treatment by BNCT, before and during neutron irradiation, the [10]B-loaded medicine (in this article, Borono-phenyl-alanine: BPA is assumed), which preferentially accumulates in tumor cells compared with normal cells, is infused. The prescribed dose is determined by the difference of accumulation between tumor and normal (T/N ratio) cells and the boron concentration in the blood of a patient. The accumulation of BPA is detected by using the PET analysis with the BPA labeled by ^{18}F nuclei. Whether the treatment case is adopted for BNCT or not, the T/N ratio is derived from PET analysis. In the KURRI protocol, the case with a T/N ratio of larger than 2.5 is adopted for BNCT.

The relative biological effectivenesses (RBEs) for nitrogen, hydrogen and gamma rays are 3.0, 3.0 and 1.0, respectively. The compound biological effectivenesses (CBEs) for tumor and normal

brain are 3.8 and 1.35, respectively. For evaluating effectiveness of treatment, the T/N ratios of 2.5, 3.5 and 4.5 were selected. The therapeutic time is determined by the dose limit for the normal brain of 10 Gy-eq.

Fig. 9 shows the distribution of biological effect weighted dose in the phantom as a function of the phantom depth. The boron concentration is assumed to be 24 ppm. In the condition of all T/N ratios, the RBE dose distribution of KUR is better than that of CBNS until a depth of 4 cm. On the other hand, at a position deeper than 4 cm, the accelerator exhibits better properties than KUR.

Figs. 10–12 show AD, AD30, and the therapeutic time as a function of the boron concentration in blood. In the case of the T/N ratios of 2.5, 3.5 and 4.5, AD of the accelerator is larger than that of KUR. For every boron concentration, CBNS can prescribe the dose at a 5–6% deeper tumor position compared with KUR.
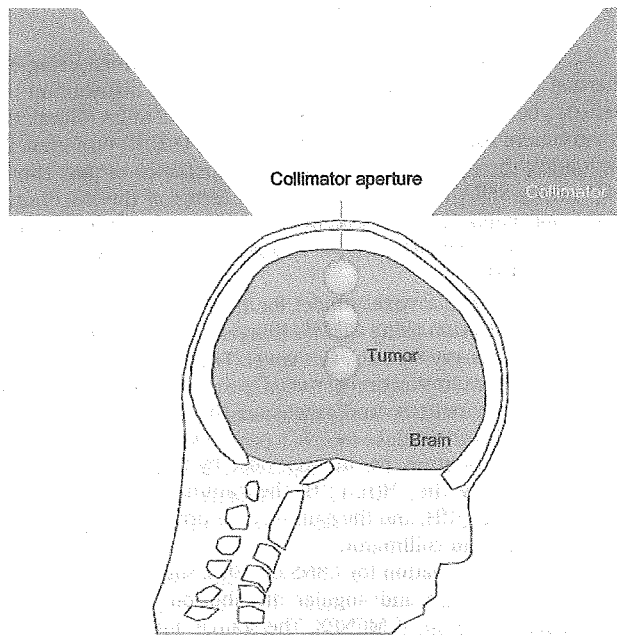

Fig. 8. Schematic image of the irradiation of brain tumor using head phantom.
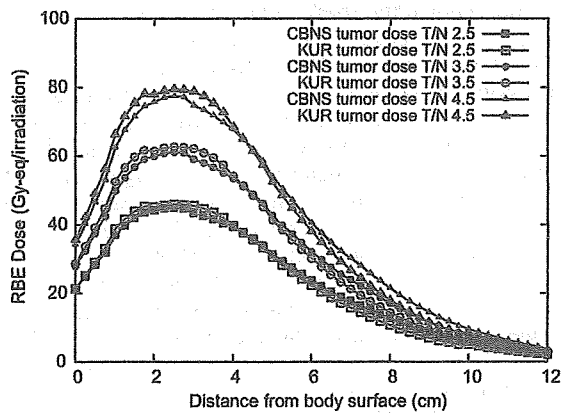
Fig. 9. Relationship between the biological effect weighted dose and the depth in head phantom.
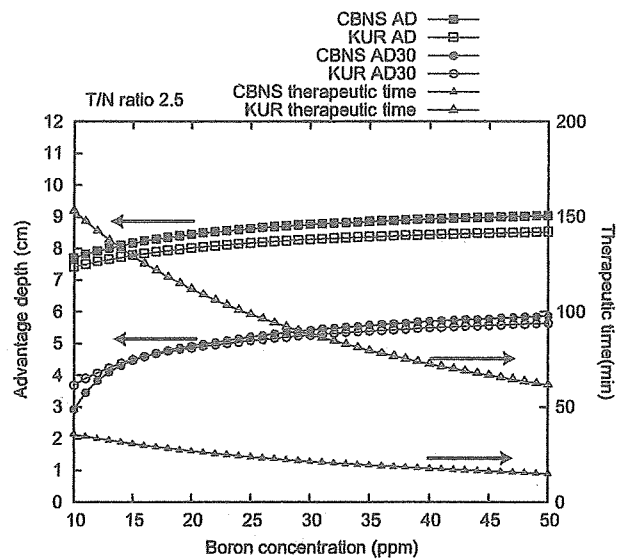

Fig. 10. Relationship of AD, AD30 Gy-eq and therapeutic time as a function of boron concentration in blood for T/N ratio of 2.5.
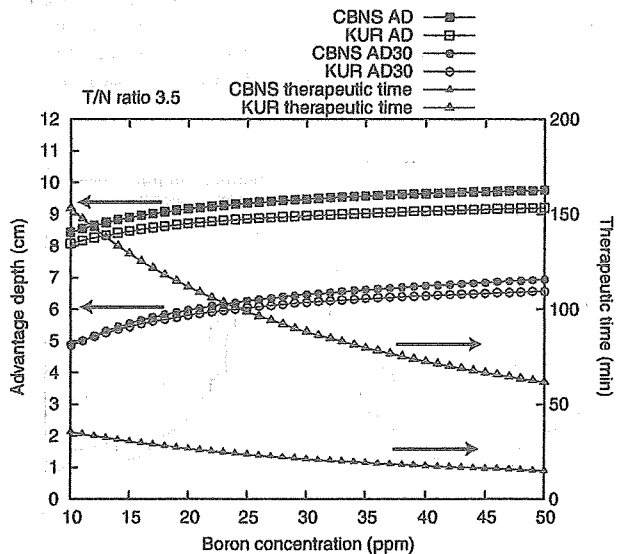

Fig. 11. Relationship of AD, AD30 Gy-eq and therapeutic time as a function of boron concentration in blood for T/N ratio of 3.5.
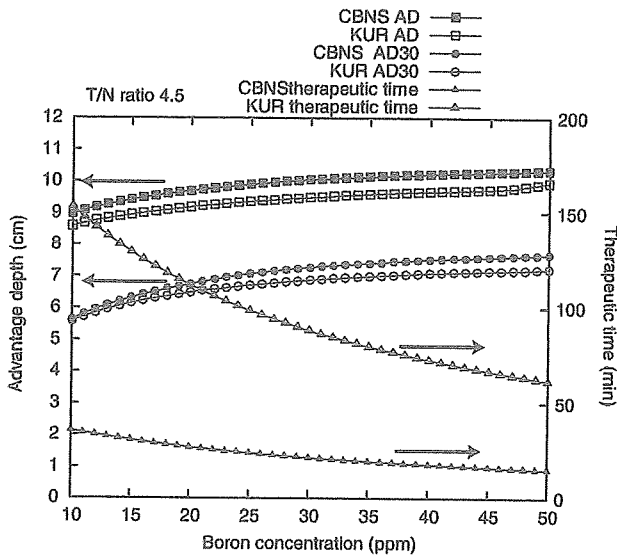
Fig. 12. Relationship of AD, AD30 Gy-eq and therapeutic time as a function of boron concentration in blood for T/N ratio of 4.5.
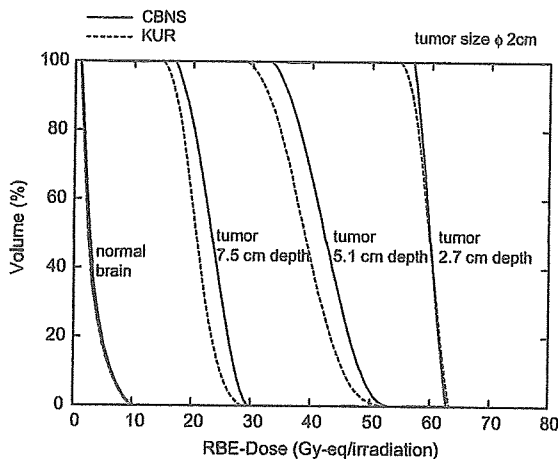

Fig. 13. Dose-volume histograms for the tumors, located at 2.7, 5.1 and 7.5 cm depth distance from head surface, and normal brain.

The superiority of CBNS for AD30 is indicated by the larger T/N ratio and higher boron concentration. For example, AD30s of CBNS at the boron concentrations of 12, 24 and 36 ppm and the T/N ratio of 3.5 are increased by 0.5%, 3.4% and 4.5% compared with KUR.

On the other hand, in the case of the T/N ratio of 2.5 shown in Fig. 10, AD30 of KUR is larger than that of CBNS with the boron of concentration of 15 ppm. This result is caused by the opposite dose distribution at a shallower depth in the phantom. The therapeutic time of the accelerator is one-quarter of that of KUR.

3.2. Dose-volume histogram analysis

Dose-volume histogram (DVH) analysis is performed for the actual treatment to evaluate the beam properties. The irradiation condition shown in Fig. 8 of the 2-cm-diameter tumors located at the depths of 2.7, 5.1 and 7.5 cm is assumed. The collimator aperture diameter is 10 cm; the boron concentration and T/N ratio are 24 ppm and 3.5, respectively.

The mean normal brain doses for KUR and the accelerator, when the maximum dose is 10 Gy-eq, are 2.5 and 2.6 Gy-eq, respectively.

In Fig. 13, the dose distribution of normal brain revealed by DVH for KUR is similar to that for the accelerator. For the tumor located at the depth of 2.7 cm, the tumor dose distributions for KUR and the accelerator almost overlap. The mean tumor dose of the accelerator for the tumors located at the depths of 5.1 cm and 7.5 cm are, respectively 10% and 18% larger than those of KUR. These results also indicated the effectiveness of the accelerator for treating deeply situated tumors using the DVH analysis.

4. Conclusion

BSA is optimized for Be targets and cyclotron-based epithemal-neutron sources by Monte Carlo simulation. With regard to the dose contamination caused by the fast neutrons and gamma rays present in the treatment beam, CBNS is superior to the present KUR facility. The evaluation of the dose distribution in a phantom revealed that AD and AD30 of CBNS with the boron concentration of 10–50 ppm and the T/N ratios of 2.5, 3.5 and 4.5 are superior to those of KUR, except for the following conditions of AD30. AD30 of KUR under the limited conditions such as a boron concentration of less than 15 ppm and the T/N ratio of 2.5 is better that of CBNS.

At KURRI, we aim to establish CBNS, which is now under construction, by 2009. KUR also will restart in the middle of 2009. KURRI has the ractor- and accelerator-based neutron sources for BNCT. KURRI is the unique facility in the world. The treatment using CBNS will be performed on the basis of the optimization presented in this article. The accelerator-based neutron source can be located near the hospital; this work could lead to the future development of BNCT.

References

[1] Minoru Suzuki, Yoshinori Sakurai, Satoru Hagiwara, Shinichiro Masunaga, Yuko Kinashi, Kenji Nagata, Akira Maruhashi, Koji Ono, First attempt of boron neutron capture therapy (BNCT) for hepatocellular carcinoma, Jpn. J. Clin. Oncol. 37 (5) (2007) 376.

[2] Minoru Suzuki, Yoshinori Sakurai, Shinichiro Masunaga, Yuko Kinashi, Kenji Nagata, Akira Maruhashi, Koji Ono, Feasibility of boron neutron capture therapy (BNCT) for malignant pleural mesothelioma from a viewpoint of dose distribution analysis, Int. J. Radiat. Oncol. Biol. Phys. 66 (5) (2006) 1584.

[3] Shunshke Yonai, Takao Aoki, Takashi Nakamura, Hiroshi Yashima, Mamoru Baba, Hitoshi Yokobori, Yoshihisa Tahara, Feasibility study on epithermal neutron field for cyclotron-based boron neutron capture therapy, Med. Phys. 30 (8) (2003) 2021.

[4] Yoshihisa Tahara, Yasushi Oda, Takako Shiraki, Takehiko Tsutsui, Hitoshi Yokobori, Shunsuke Yonai, Mamoru Baba, Takashi Nakamura, Engineering design of a spallation reaction-based neutron generator for boron neutron capture therapy, J. Nucl. Sci. Technol. 43 (1) (2006) 9.

[5] MCNPX User's Manual Version 2.4.0, LA-CP-02-408, Los Alamos National Laboratory (LANL), 2002.

[6] R.E. Prael, H. Lichtenstein, User Guide to LCS: The LAHET Code Systems, LA-UR-89-3014, Los Alamos National Laboratory, 1989.

[7] Takahiro Tadokoro, Yukio Kawakubo, Hirofumi Seki, Ryuichi Tayama, Kikuo Umegaki, Mamoru Baba, Tooru Kobayashi, Feasibility study on a common use accelerator system of neutron production for BNCT and radionuclide production for PET, in: Advances in Neutron Capture Therapy 2006 (Proceedings of the ICNCT-12), 2006, p. 304 .

[8] S. Tanaka, M. Fukuda, K. Nishimura, et al., A code system to calculate induced radioactivity produced by ions and neutrons, JAERI-Data/Code 97-019, 1997.

[9] J.C. Yanch, X.L. Zhou, G.L. Brownell, A Monte Carlo investigation of the dosimetric properties of monoenergetic neutron beams for neutron capture therapy, Radiat. Res. 126 (1991) 1.

[10] Y.W.H. Liu, T.T. Huang, S.H. Jiang, H.M. Liu, Renovation of epithermal neutron beam for BNCT at THOR, Appl. Radiat. Isotop. 61 (2004) 1039.

[11] Yoshinori Sakurai, Tooru Kobayashi, Characteristics of the KUR heavy water neutron irradiation facility as a neutron irradiation field with variable energy spectra, Nucl. Instr. and Meth. A 453 (2000) 569.

[12] ICRP Publication 74, Conversion Coefficients for Use in Radiological Protection Against External Radiation, 1996.

[13] D. Wessol, M. Cohen, G. Harkin, M. Rossmeier, C. Wemple, F. Wheeler, in: SERA Workshop Lab Manual, INEEL/EXT-99-00766, 1999.

[14] D.W. Nigg, C.A. Wemple, D.E. Wessol, F.J. Wheeler, SERA-an advanced treatment planing system for neutron capture therapy and BNCT, Trans. Am. Nucl. Soc. 80 (1999) 66.

[15] Yoshinori Sakurai, Koji Ono, Improvement of dose distribution by central beam shielding in boron neutron capture therapy, Phys. Med. Biol. 52 (2007) 7409.
[16] R. Mayer, P. Sminia, Reirradiation tolerance of the human brain, Int. J. Radiat. Oncol. Biol. Phys. 70 (2008) 1350.
[17] J.F. Fowler, W.A. Tome, J.D. Fenwick, M.P. Mehta, A challenge to traditional radiation oncology, Int. J. Radiat. Oncol. Biol. Phys. 60 (2004) 1241.

[18] G.E. Laramore, F.J. Wheeler, D.E. Wessol, K.J. Stelzer, T.W. Griffin, A tumor control curve for malignant gliomas derived from fast neutron radiotherapy data: implications for treatment delivery and compound selection, advances in neutron capture therapy, in: Proceedings of the Seventh International Symposium on Neutron Capture Therapy for Cancer, 2007, p. 580.
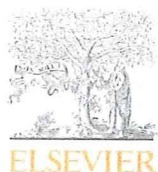
Improvement of dose distribution in phantom by using epithermal neutron source based on the Be(p,n) reaction using a 30 MeV proton cyclotron accelerator

H. Tanaka [a,*], Y. Sakurai [a], M. Suzuki [a], T. Takata [a], S. Masunaga [a], Y. Kinashi [a], G. Kashino [a], Y. Liu [a], T. Mitsumoto [b], S. Yajima [b], H. Tsutsui [b], M. Takada [c], A. Maruhashi [a], K. Ono [a]

[a] Research Reactor Institute, Kyoto University, Asashiro-nishi 2-1010, Kumatori-cho, Osaka 590-0494, Japan
[b] Sumitomo Heavy Industries, Osaki 2-1-1, Shinagawa, Tokyo 141-6025, Japan
[c] National Institute of Radiological Sciences, Anagawa 4-9-1, Inage-ku, Chiba-shi 263-8555, Japan

ARTICLE INFO

ABSTRACT

In order to generate epithermal neutrons for boron neutron capture therapy (BNCT), we proposed the method of filtering and moderating fast neutrons, which are emitted from the reaction between a beryllium target and 30 MeV protons accelerated by a cyclotron, using an optimum moderator system composed of iron, lead, aluminum, calcium fluoride, and enriched ^{6}LiF ceramic filter. At present, the epithermal-neutron source is under construction since June 2008 at Kyoto University Research Reactor Institute. This system consists of a cyclotron to supply a proton beam of about 1 mA at 30 MeV, a beam transport system, a beam scanner system for heat reduction on the beryllium target, a target cooling system, a beam shaping assembly, and an irradiation bed for patients.

In this article, an overview of the cyclotron-based neutron source (CBNS) and the properties of the treatment neutron beam optimized by using the MCNPX Monte Carlo code are presented. The distribution of the RBE (relative biological effectiveness) dose in a phantom shows that, assuming a ^{10}B concentration of 13 ppm for normal tissue, this beam could be employed to treat a patient with an irradiation time less than 30 min and a dose less than 12.5 Gy-eq to normal tissue. The CBNS might be an alternative to the reactor-based neutron sources for BNCT treatments.

© 2009 Elsevier Ltd. All rights reserved.

1. Introduction

At first, the BNCT treatments using KUR (Kyoto University Research Reactor) were adapted for malignant melanoma and brain tumors. The widespread application to the treatment of other diseases such as recurrent head and neck tumors, liver tumors (Suzuki et al., 2007), and mesothelioma (Suzuki et al., 2006) using epithermal neutrons, has resulted in an increased number of clinical trials. In order to obtain good results for deep tumors, a higher dose is required. Moreover, a sufficient neutron yield obtained by using an accelerator-based neutron source that can be located near a hospital would be useful for further developments of BNCT.

Yonai et al. (2003) and Tahara et al. (2006) are already investigating a neutron source using spallation reactions that occur for 30–50 MeV protons incident on a tantalum target. The possibility of exploiting the reaction of several tens of MeV protons incident on a beryllium target, was excluded because of the fast neutrons contamination of the treatment beam. However, a sufficient epithermal neutron yield based on the Be(p,n) reaction could be obtained with an optimum beam-shaping assembly. Our system has the advantage of a larger neutron yield and a lower activation of the target material in comparison with the spallation reactions involving heavy materials.

The neutron transport for optimum treatment beams was simulated by using the Monte Carlo calculation code MCNPX (Pelowitz, 2005). This article reports an overview of the epithermal neutron generator and calculated parameters in phantom.

2. Material and methods

2.1. Cyclotron accelerator and beryllium target

The cyclotron accelerator (HM-30) manufactured by Sumitomo Heavy Industries is employed to provide a ~1 mA, 30 MeV proton beam. In the HM-30 hydrogen negative ions are accelerated and protons up to 30 MeV are derived by charge conversion in a carbon

* Corresponding author.
E-mail address: h-tanaka@rri.kyoto-u.ac.jp (H. Tanaka).

Table 1
Target material properties for Be, Ta and W.

Target	Melting point (deg)	Boiling point (deg)	Thermal conductivity ($W m^{-1} K^{-1}$)	Neutron yield ($sec^{-1} mA^{-1}$)	Gamma ray yield per one neutron
Be	1278	2970	201	1.90×10^{14}	0.02
Ta	3017	5458	57.5	1.27×10^{14}	0.93
W	3422	5555	174	9.65×10^{13}	1.40

foil stripper. The proton beam derived from HM-30 is led to a beryllium target via a beam transport system. A uniform 120 mm × 120 mm proton beam at the beryllium target is shaped by a controlling magnetic field of two scanning magnets.

Table 1 shows the characteristics of Be, W, and Ta target materials when irradiated by a 1 mA, 30 MeV proton beam. The neutron and gamma ray yields were estimated by using the MCNPX code and the cross-section data of ENDF/B-VII, physical model, and la150 for Be, Ta, and W, respectively. In comparison with the other materials listed in Table 1, Be shows the highest neutron yield, the smallest gamma-ray yield per neutron, the highest thermal conductivity, and a high melting point. A 1 mA, 30 MeV proton beam has a 30 kW power. Such a large heat input needs a target-cooling system. In our system, a Be target is directly cooled by pure compressed water. The compressed water flows through a spiral water channel. 30 MeV protons with a range of 5.8 mm in Be penetrate a 5.5 mm-thick Be target and inject in the compressed cooling water in order to prevent blistering of the target.

With regard to the experimental results for the thermal resistance of a Be target, Tadokoro et al. (2006) indicated that a heat input of 500 W/cm² leads to a temperature less than 500 °C. The irradiation area should be expanded to 60 cm² for a heat input of 500 W/cm² under 30 kW operation. The area of 144 cm² scanned by two scanning magnets is sufficient for heat reduction on the target.

In order to evaluate the target activation resulting from 1 year of operation a 2 h irradiation per day with a 1 mA proton current was assumed. The neutron- and proton-induced activation of the three above materials was calculated by using the IRACM code (Tanaka et al., 1997). The nuclei produced in a W target have higher activity and longer half lives than Be and Ta targets. Immediately after the daily operation, the activation rate of a Ta target is four orders of magnitude higher than that of a Be target. The period required for the Ta target until the ambient dose rate becomes 1 mSv h⁻¹ is twice of that required for the Be target. Considering the above-mentioned results in terms of neutron yield, thermal properties, and activation level, the Be target was chosen.

2.2. Beam-shaping assembly (BSA)

Yanch et al. (1991) found out that for BNCT treatments at a 10 cm depth in the head, the most effective neutron energy is 10 keV and the most effective neutron energy range is between 4 eV and 40 keV.

In the reaction between 30 MeV protons and a Be target, the neutrons that are emitted in the forward direction have an energy of up to 28 MeV. In order to reduce the neutron energy to the epithermal energy range, a BSA composed of a moderator and a shaper has been employed. The moderator is used to reduce the energy from the maximum value of 28 MeV with low capture cross-section. The shaper is used to obtain the 10 keV optimum energy mentioned above.

Fig. 1 shows the schematic layout of the BSA. The moderator materials are Pb and Fe. The Pb component, used as a breeder and a reflector for high energy neutrons, was installed near the target.
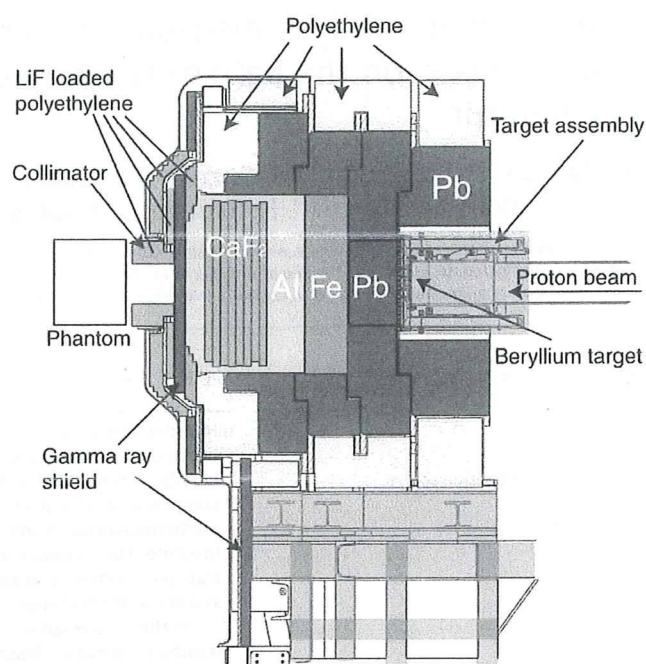

Fig. 1. Schematic layout of the BSA to obtain an epithermal neutron beam using a 30 MeV proton beam incident on a beryllium target.

The Fe component, mainly used as a moderator, was installed after the Pb component. With regard to the shaper, AlF₃ is often used in the design of an epithermal neutron generator (Liu et al., 2004; Culbertson et al., 2004) and the material density should be high in order to form a compact BSA. It is difficult to increase the AlF₃ density because it sublimes at a temperature of 1040 °C under atmospheric pressure. Therefore, we focused on Al and CaF₂ instead of AlF₃.

The optimum thickness of each component was determined through the calculation of the dose distribution in the phantom composed of soft average tissue of an adult male (ICRU-44) by using the MCNPX code.

In order to prevent the exposure of the patient to the fast-neutron radiation, the moderator, the shaper, and the front surface of the collimator are surrounded by polyethylene blocks.

Furthermore, in order to accurately set the patient in the position determined by the treatment planning system, an X-ray tube and an imaging plate are installed. The pair of X-ray tube and imaging plate can be moved to the neutron beam side and an image of the "beam's eye view" can be obtained. Laser markers are also installed; the irradiation position is set by a marking on the skin.

3. Results and discussion

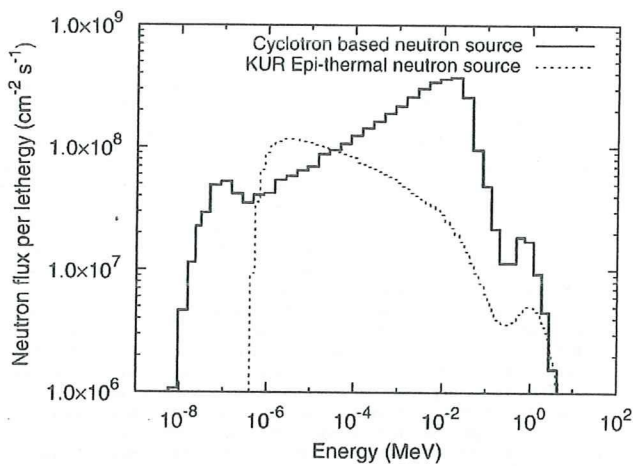All the following results are related to a 1 mA, 30 MeV proton beam.

Fig. 2. Comparison between the CBNS neutron spectrum and the KUR one.

3.1. Free beam properties

Fig. 2 shows the CBNS neutron flux spectrum under the free-air condition evaluated at the surface of the gamma-ray shield in comparison with the KUR one, which is most-often used in the BNCT treatments (Sakurai and Kobayashi, 2000). The CBNS neutron spectrum has a peak in the 10–20 keV energy range.

In some of the BNCT literature, the epithermal range is defined as the interval from 0.5 eV to 10 keV, which is recommended by IAEA-TECDOC1223 (2001). However, we designed the moderator to fulfill the maximization of epithermal neutron flux with the interval from 4 eV to 40 keV, which is more effective to treat deep tumors. Furthermore, Blue et. al. (1993) showed the calculated RBE value as a function of neutron energy and found out that the RBE of the energy of 40 keV was less than 3.0. They also showed the RBE of the energy of around 0.5 eV was less than 3.0. It is appropriate to define the value of 40 keV as boundary energy between epithermal and fast neutron. Consequently, in this article, the definition of the epithermal energy range is from 0.5 eV to 40 keV. The energy region below 0.5 eV is defined as the thermal region; that above 40 keV, as the fast-neutron region.

The fast-neutron and gamma-ray dose contaminations per epithermal neutron for CBNS under the free-air condition are 5.84×10^{-13} and 7.75×10^{-14} Gy cm^2, respectively. Each absorbed dose value was obtained by using the neutron flux at the gamma-ray shield and the flux-to-dose conversion factors published in ICRP-74. The human tissue components were assumed to be H: 11.1, C: 12.6, N: 2.0, and O: 74.3 (wt%). The fast-neutron and gamma-ray dose contaminations per epithermal neutron for KUR under the free-air condition are 9.10×10^{-13} and 2.40×10^{-13} Gy cm^2, respectively (Sakurai and Kobayashi, 2000). With regard to the fast neutrons and gamma rays contaminations the CBNS facility is superior to KUR one.

3.2. Beam characteristics in phantom

Fig. 3 shows the evaluation of the CBNS neutron flux components in a phantom located in front of the collimator. The diameter of the collimator aperture and phantom are 16 and 26 cm, respectively. The maximum value of thermal neutron flux is 2.3×10^9 cm^{-2}s^{-1} at a depth of 2.3 cm in phantom.

The prescribed dose is determined by the differential boron accumulation in tumor and normal cells (T/N ratio) and the boron concentration in the blood of the patient. The RBEs assumed for nitrogen, hydrogen, and gamma rays are 3.0, 3.0, and 1.0,
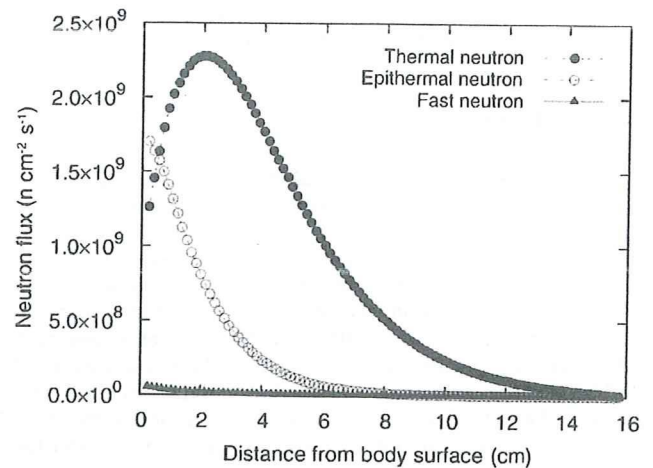

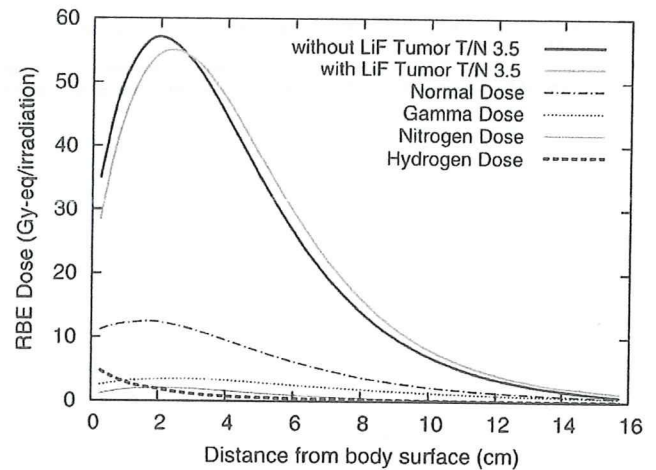Fig. 3. Neutron flux components (thermal, epithermal and fast) in phantom.

Fig. 4. RBE dose components in phantom.

respectively. The compound biological effectiveness (CBE) factors for tumor and normal brain are 3.8 and 1.35, respectively. The T/N ratio of 3.5 is employed. The boron concentration is assumed to be 13 ppm. The therapeutic time is determined by the dose limit for the normal brain of 12.5 Gy-eq. Fig. 4 shows the distribution of the RBE dose components in the phantom. Under the above hypotheses, the RBE dose in tumor reaches a maximum value of 57 Gy-eq at a depth of about 2.3 cm in phantom and the irradiation time is less than 30 min. The sufficient dose for killing the tumor is at least 30 Gy-eq. The CBNS facility can treat a tumor located within a depth of 5.5 cm, with the RBE dose of 30 Gy-eq by single irradiation. With regard to the irradiation of deeper tumors, the bilateral irradiation can be adopted to raise the prescribed dose. At a depth of 8 cm, the RBE dose is about 15 Gy-eq. Therefore CBNS can treat tumors situated at almost all the positions in the brain by using the bilateral irradiation.

Furthermore, to improve the dose distribution at a deeper position, an enriched ^{6}LiF ceramic filter (thickness of 6 mm) placed after the gamma ray shield can be used. The enriched ^{6}LiF filter produces a more ideal neutron spectrum because of filtering in the low energy region. The thickness of ^{6}LiF filter is optimized to fulfill a therapeutic time of less than 60 min. Fig. 4 shows the dose distribution in phantom using the enriched ^{6}LiF ceramic

filter. The use of this filter increases the treatable depth from 5.5 to 6.0 cm with the RBE dose of 30 Gy-eq.

4. Conclusions

By means of Monte Carlo simulations a moderator and a shaper have been optimized for the high energy neutrons emitted from the Be(p,n) reaction with a 1 mA, 30 MeV proton beam. With regard to the fast neutrons and gamma rays dose contamination, CBNS is superior to the current KUR facility. From the evaluation of the dose distribution in a phantom the irradiation time using CBNS turns out to be about 30 min. CBNS becomes a powerful tool for treating deep tumors by using the bilateral irradiation. The CBNS facility is now under construction and the aim is to establish it at KURRI by 2009. KUR also will restart in the middle of 2009. Thus KURRI will have both the reactor- and the accelerator-based neutron sources for BNCT.

References

Blue, T.E., Gupta, N., Woollard, J.E., 1993. A calculation of the energy dependence of the RBE of neutrons. Phys. Med. Biol. 38, 1693–1712.

Culbertson, C.N., Green, S., Mason, A.J., Picton, D., Baugh, G., Hugtenburg, R.P., Yin, Z., Scott, M.C., Nelson, J.M., 2004. In-phantom characterisation studies at the Birmingham accelerator-generated epithermal neutron source (BAGINS) BNCT facility. Appl. Radiat. Isot. 61, 733–738.

IAEA TECDOC 1223, 2001. Current status of neutron capture therapy.

Liu, Y.W.H., Huang, T.T., Jiang, S.H., Liu, H.M., 2004. Renovation of epithermal neutron beam for BNCT at THOR. Appl. Radiat. Isot. 61, 1039–1043.

Pelowitz, D.B., 2005. MCNPX user's manual—version 2.5.0. Los Alamos National Laboratory Report LA-CP-05-0369.

Sakurai, Y., Kobayashi, T., 2000. Characteristics of the KUR heavy water neutron irradiation facility as a neutron irradiation field with variable energy spectra. Nucl. Instrum. Methods A 453, 569–596.

Suzuki, M., Sakurai, Y., Masunaga, S., Kinashi, Y., Nagata, K., Maruhashi, A., Ono, K., 2006. Feasibility of boron neutron capture therapy (BNCT) for malignant pleural mesothelioma from a viewpoint of dose distribution analysis. Int. J. Radiat. Oncol. Biol. Phys. 66 (5), 1584–1589.

Suzuki, M., Sakurai, Y., Hagiwara, S., Masunaga, S., Kinashi, Y., Nagata, K., Maruhashi, A., Ono, K., 2007. First attempt of boron neutron capture therapy (BNCT) for hepatocellular carcinoma. Jpn. J. Clin. Oncol. 37 (5), 376–381.

Tadokoro, T., Kawakubo, Y., Seki, H., Tayama, R., Umegaki, K., Baba, M., Kobayashi, T., 2006. Feasibility study on a common use accelerator system of neutron production for BNCT and radionuclide production for PET. Advances in neutron capture therapy 2006. In: Proceedings of ICNCT-12, pp. 304–307.

Tahara, Y., Oda, Y., Shiraki, T., Tsutsui, T., Yokobori, H., Yonai, S., Baba, M., Nakamura, T., 2006. Engineering design of a spallation reaction-based neutron generator for boron neutron capture therapy. J. Nucl. Sci. Technol. 43 (1), 9–19.

Tanaka, S., Fukuda, M., Nishimura, K., 1997. A code system to calculate induced radioactivity produced by ions and neutrons. JAERI-Data/Code 97-019.

Yanch, J.C., Zhou, X.L., Brownell, G.L., 1991. A Monte Carlo investigation of the dosimetric properties of monoenergetic neutron beams for neutron capture therapy. Radiat. Res. 126, 1–20.

Yonai, S., Aoki, T., Nakamura, T., Yashima, H., Baba, M., Yokobori, H., Tahara, Y., 2003. Feasibility study on epithermal neutron field for cyclotron-based boron neutron capture therapy. Med. Phys. 30 (8), 2021–2030.

A Simple and Rapid Method for Measurement of 10B-*para*-Boronophenylalanine in the Blood for Boron Neutron Capture Therapy Using Fluorescence Spectrophotometry

Genro KASHINO[1], Satoshi FUKUTANI[2], Minoru SUZUKI[1], Yong LIU[1],
Kenji NAGATA[1], Shin-Ichiro MASUNAGA[1], Akira MARUHASHI[1],
Hiroki TANAKA[3], Yoshinori SAKURAI[3], Yuko KINASHI[4],
Noriko FUJII[5] and Koji ONO[1]*

Boron/Neutron/Capture/Therapy.

Background and Purpose; 10B deriving from 10B-*para*-boronophenylalanine (BPA) and 10B-borocaptate sodium (BSH) have been detected in blood samples of patients undergoing boron neutron capture therapy (BNCT) using prompt gamma ray spectrometer or Inductively Coupled Plasma (ICP) method, respectively. However, the concentration of each compound cannot be ascertained because boron atoms in both molecules are the target in these assays. Here, we propose a simple and rapid method to measure only BPA by detecting fluorescence based on the characteristics of phenylalanine. *Material and Methods;* 10B concentrations of blood samples from human or mice were estimated by the fluorescence intensities at 275 nm of a BPA excited by light of wavelength 257 nm using a fluorescence spectrophotometer. *Results;* The relationship between fluorescence to increased BPA concentration showed a positive linear correlation. Moreover, we established an adequate condition for BPA measurement in blood samples containing BPA, and the estimated 10B concentrations of blood samples derived from BPA treated mice were similar between the values obtained by our method and those by ICP method. *Conclusion;* This new assay will be useful to estimate BPA concentration in blood samples obtained from patients undergoing BNCT especially in a combination use of BSH and BPA.

INTRODUCTION

10B-*para*-boronophenylalanine (BPA) and 10B-borocaptate sodium (BSH) have been used for boron neutron capture therapy (BNCT).[1-5] 10B nucleus has markedly large cross section to capture slow neutrons in comparison with body composition elements. The 10B (n, α) 7Li reaction releases a high linear energy transfer (LET) α particle and a recoiling 7Li ion with an average total kinetic energy of 2.34 MeV.

Their tracks do not exceed one cell diameter. Therefore if these compounds accumulate in tumour cells or tumour tissue and they receive thermal neutrons or epi-thermal neutrons, the tumours can be destroyed efficiently and selectively. As the effectiveness of BNCT is related primarily to the selective accumulation of the boron compounds in the tumor relative to the surrounding normal tissues, concentration of boron compounds should be monitored carefully for efficient killing of the tumour cells. In the clinical setting of BNCT, the 10B concentration in blood should be monitored to estimate radiation dose delivered to tumour and normal tissues. As previously reported, BPA and BSH are combined to ensure such efficient killing.[6-10] The relative BNCT effect varies depending on the combination of 10B compound and tissue or organ even at a same 10B concentration and neutron fluence. This effective RBE has been determined by experiments on each normal tissue assuming that 10B compound is distributing in the tissue at equal concentration in blood. 10B concentration in blood has been measured by prompt gamma ray spectrometer, or ICP method.[11-13] However,

these methods can not distinguish ^{10}B concentration of BPA and BSH in blood samples. Therefore, a simple and rapid method to measure ^{10}B concentration of each compound separately is needed to accurately estimate X-ray equivalent dose. We proposed a simple and rapid method to measure only BPA by detecting fluorescence at 275 nm of a BPA compound excited by light of wavelength 257 nm using a fluorescence spectrophotometer based on the characteristics of phenylalanine.

MATERIALS AND METHODS

Measurement of BPA concentration in ethanol

A stock solution of BPA (1,300 or 1,600 ppm ^{10}B) was used for all experiments. BPA solutions were diluted with ethanol, and 1 ml solution was poured into the cuvette and placed in the cell of the fluorescence spectrophotometer (F-2000; Hitachi, Tokyo, Japan). The fluorescence spectrophotometer was set at 700 V for detection amplification. Excitation and emission wavelengths were 257 nm and 275 nm, respectively. These wavelengths were determined from the fact that phenylalanine can be measured in these wavelength with little influence by the other amino acids such as tyrosine and tryptophan.[14] This was evidenced in Fig 2a.

Measurement of BPA concentration in human blood

Blood samples obtained from a healthy man volunteer (35 years old) was analysed within 24 h. An aliquot of 200 μl of blood was added to each 1.5 ml tube, and 1–10 μl of BPA (6.5–65 ppm ^{10}B) and 1.2 μl of BSH (30 ppm ^{10}B) stock solution were added to the blood samples. After vortex-mixing the sample for a few seconds, blood was centrifuged at 15,000 rpm for 2 minutes, and 50 μl of the supernatant containing plasma fraction was poured in another 1.5 ml tube. A 12-fold volume of ethanol (600 μl) was added to the plasma and the tube was vortex-mixed. Samples were centrifuged at 15,000 rpm for 2 minutes. After centrifugation, supernatants were poured into the collection tube, which was part of a syringeless filter device (Mini-Uniprep, Whatman, NJ, USA). The solution was pushed through polytetrafluoroethylene filter media (pore size, 0.45 μm) to remove proteins present in the plasma solution. Filtrated solutions were diluted with ethanol to concentrations (10-, 20- and 25-fold), and 1 ml solutions were poured into the cuvette and placed in the cell of the fluorescence spectrophotometer.

Measurement of BPA concentration in mice blood

BPA solution (0.3 or 0.6 ml of 1,600 ppm ^{10}B) was administrated intraperitoneally to C3H mice. Twenty minutes after injection of BPA, 0.3 ml of heparin solution (1,000 unit/ml of heparin sodium solution, Ajinomoto, Tokyo, Japan) was injected. Five minutes after injection of heparin, 500–1,000 μl of blood was collected from the eye's artery. An aliquot

of 50 μl of blood was added to each 1.5 ml tube, and 0.5–1.5 μl of BPA (16–48 ppm ^{10}B) were added to the blood samples. After vortex-mixing the sample for a few seconds, blood was centrifuged at 15,000 rpm for 2 minutes, and 20 μl of the supernatant containing plasma fraction was poured in another 1.5 ml tube. A 12-fold volume of ethanol (240 μl) was added to the plasma and the tube was vortex-mixed. Samples were centrifuged at 15,000 rpm for 2 minutes. After centrifugation, supernatants were poured into the collection tube, which was part of a syringeless filter device (Mini-Uniprep, Whatman, NJ, USA). The solution was pushed through polytetrafluoroethylene filter media (pore size, 0.45 μm) to remove proteins present in the plasma solution. Filtrated solutions were diluted with ethanol to concentrations (20-fold), and 1 ml solutions were poured into the cuvette and placed in the cell of the fluorescence spectrophotometer.

ICP method

Plasma samples were obtained after centrifugation of human and mice blood as described previously. Twenty micro-litter of plasma were diluted with 5 ml water and stored in the fridge. Inductively Coupled Plasma (ICP) method was performed as following the recommended instruction. The concentration of boron in each plasma sample was determined by ICPS-1000TR (Shimazu, Kyoto, Japan).

RESULTS AND DISCUSSION

The relationship between BPA concentration in ethanol and fluorescence showed a positive linear correlation until high intensities of fluorescence were achieved (Fig. 1). Our measurement condition was therefore suitable for detecting
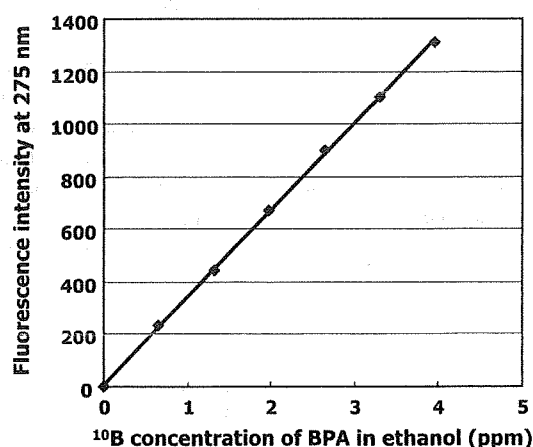

Fig. 1. Relationship between BPA concentration and fluorescence intensity at 275 nm in ethanol. The fluorescence value of only ethanol was subtracted at all points. The equation of this line was $y = 332 x + 9.26$ ($R^2 = 0.9996$).

BPA concentration without fluorescence saturation. A similar slope for the scattered plot was obtained if water or phosphate-buffered solution was used instead of ethanol as the solvent (data not shown), suggesting that soluble BPA was detected without the influence of solvents. Ethanol, even in the absence of BPA, emits fluorescence at 275 nm after excitation by light at 257 nm. The value for ethanol without BPA was 130–180 and the obtained fluorescence value of only ethanol was subtracted from the total fluorescence value of BPA and ethanol solution.

Despite the influences of many fractions in blood, only BPA should be measured in this method. The fluorescence spectrum between 260 and 360 nm excited by the light

257 nm were shown in Fig 2a. The spectrums for the samples derived from human plasma without BPA (dark blue) were clearly different from the spectrum for ethanol only. This suggests that plasma only emit the light (especially in over 280 nm). However, the light 275 nm were not influenced by the fractions of plasma and increased intensities in 275 nm were observed with higher concentration of BPA (Fig 2a). The scattered plots of the samples derived from human blood before subtraction of the ethanol intensities and after subtraction of those were shown on the left (b) and right (c) of Fig. 2, respectively. In the sample without BPA addition (0 ppm), fluorescence was the same as the intensity of ethanol when used alone (zero in Fig. 2c), suggesting that
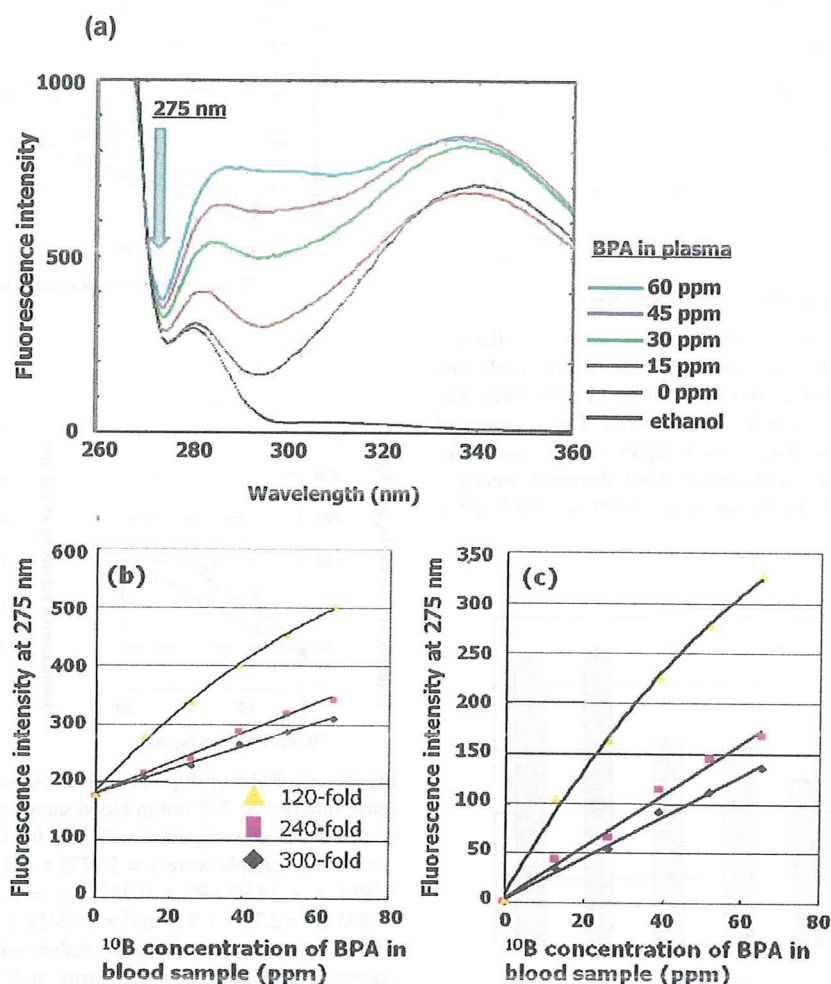

Fig. 2. (a) The fluorescence spectrum between 260 and 360 nm excited by the light 257 nm in BPA added plasma samples. (b)(c) Relationship between BPA concentration and fluorescence intensity at 275 nm in blood samples. (b) Scattered plots before subtraction of the fluorescence value for only ethanol, and (c) after subtraction of the fluorescence value for only ethanol. The data from the three ratios for dilution of blood samples are represented as follows: 120-fold: yellow triangle; 240-fold: pink square and 300-fold: blue diamond. The equations of lines for the scattered plots from 120-, 240- and 300-fold dilution were $y = -0.0303 x^2 + 6.82 x + 183.24$ ($R^2 = 0.9968$), $y = 2.5963 x + 178.87$ ($R^2 = 0.9908$) and $y = 2.0538 x + 178.33$ ($R^2 = 0.9929$), respectively.

all other components which influence measurement at 275 nm were excluded by our treatments. When the samples were prepared for measurement, plasma samples were diluted with ethanol. We diluted the samples at three types of ratio. Slope values decreased according to the dilution ratio. In case of 120-fold dilution, the shape of the line was quadratic at < 65 ppm ^{10}B of BPA. The reason for as to why the scattered plots reached the ceiling at lower dilution ratio is unclear, but linear increase with 2.1 and 2.6 of slope value was observed in 300-fold and 240-fold dilution samples, respectively. This slope value means that the range of resolution is < 0.5 ppm ^{10}B in BPA containing blood sample. We therefore applied a 240-fold dilution in the further study.

To mimic the blood sample of a patient undergoing BNCT, BPA containing blood sample at 13 ppm ^{10}B was previously prepared for creating scattered plots, in addition to the control scattered plots between ^{10}B of BPA concentra-

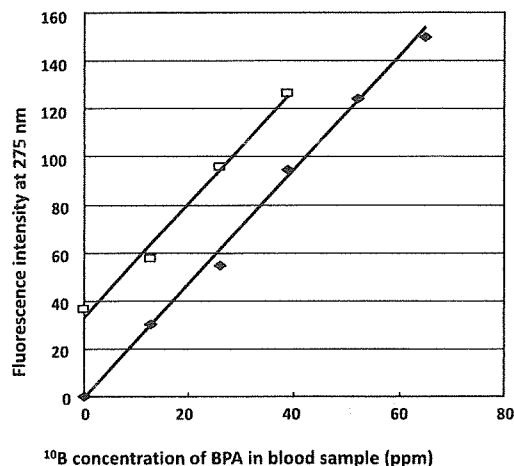
^{10}B concentration of BPA in blood sample (ppm)

Fig. 3. Relationship between BPA concentration and fluorescence intensity at 275 nm in blood samples with (white square) and without (black diamond) previous addition of 13 ppm BPA. The dilution ratio of all blood samples was 240-fold. The equations of lines for the scattered plots from blood samples with previous addition of BPA (white square) and control (black diamond) were y = 2.3654 x + 32.85 (R^2 = 0.988) and y = 2.3479 + 0.7905 (R^2 = 0.9966), respectively.
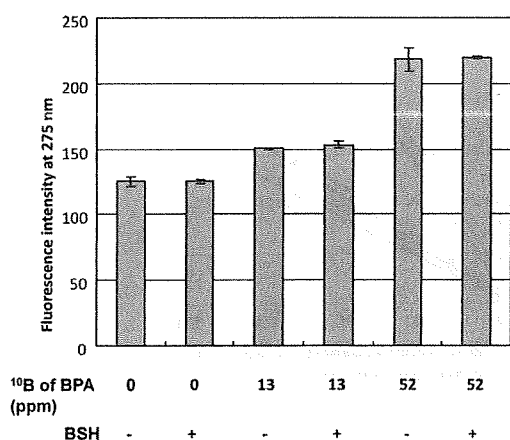

Fig. 4. Little effects were observed by the presence of BSH on BPA measurement in the blood samples. Thirty ppm ^{10}B of BSH was added to blood sample containing BPA in each concentration. Result shows mean frequency ± standard error of the mean (SEM) of fluorescence intensities from three independent experiments.

(a)

^{10}B concentration of BPA in blood sample (ppm)

(b)

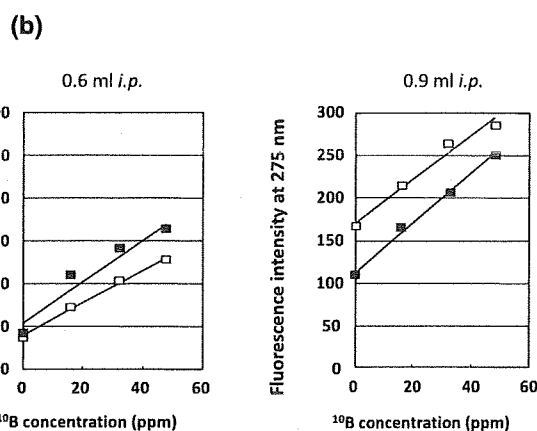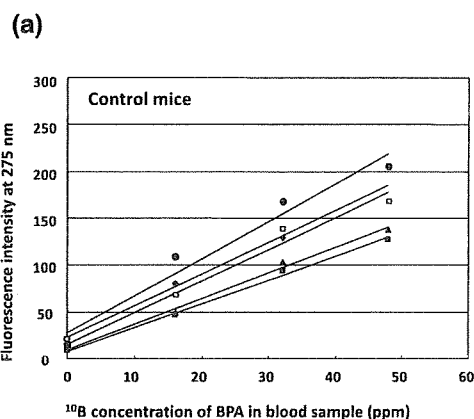^{10}B concentration (ppm) ^{10}B concentration (ppm)

Fig. 5. (a) Relationship between BPA concentration and fluorescence intensity at 275 nm in blood samples derived from five non-treated mice. The equations of lines for the scattered plots from each mouse sample were y = 3.9775 x + 27.49 (R^2 = 0.9607), y = 3.3981 x + 14.92 (R^2 = 0.9877), y = 3.3906 x + 22.55 (R^2 = 0.9965), y = 2.72 x + 9.97 (R^2 = 0.9945), y = 2.5338 x + 7.84 (R^2 = 0.9959), respectively. (b) Relationship between added BPA concentration and fluorescence intensity at 275 nm in blood samples derived from mice treated with 0.6 ml (left) and 0.9 ml (right) BPA solutions. The equations of lines for the scattered plots from the samples of 0.6 ml and 0.9 ml treated mouse were y = 2.4069 x + 54.11 (R^2 = 0.9442) (black plots of left panel), y = 1.8869 x + 39.69 (R^2 = 0.9923) (white plots of left panel), and y = 2.5719 x + 170.45 (R^2 = 0.9782) (white plots of right panel), y = 2.93 x + 112.33 (R^2 = 0.9982) (black plots of right panel), respectively.

tions and fluorescence intensities. Two nearly parallel linear scattered plots were obtained between the control and the BPA-added sample (Fig. 3). The equations of lines for the scattered plots from blood samples with previous addition of BPA (white square) and control (black diamond) were y = 2.3654 x + 32.85 (R^2 = 0.988) and y = 2.3479 x + 0.7905 (R^2 = 0.9966), respectively. Therefore, the slope value was indicated to be almost equal (2.3654 vs 2.3479). It was indicated that the increased fluorescence intensity in the sample with previous addition of BPA was 32.06 at the y intercept after subtraction of background y value. The estimated BPA concentration in the sample was 13.55 ppm (32.06 was divided by 2.3654, slope for pink plots). This estimated value is very similar with 13 ppm as an actual concentration.

Also, we examined the influence of BSH on our BPA measurement, and the result showed that no influences by the presence of 30 ppm ^{10}B of BSH were observed in the fluorescence intensities for ^{10}B of BPA (Fig. 4). It is clear that we can measure the ^{10}B concentrations of BPA by this method using blood samples simultaneously containing two compounds. In the present clinical use of BPA with BSH, approximate concentrations for each compound have been estimated by the expected concentrations for ^{10}B of BSH, which had been obtained from attenuation curve of BSH concentrations. Therefore, the results are clearly showing that an application of our method to clinical setting for BNCT will improve the measurement of ^{10}B concentrations for BPA and BSH.

To mimic the patient situation, BPA treated mice were analysed. Because of the small blood volume, we could not estimate the background intensity in a BPA treated mouse unlike in human. Therefore, we first estimated an average of background intensity from five mice. BPA was added in the

blood samples derived from five mice, and five linear lines followed by scattered plots were drawn with a good correlation (Fig. 5a). The reason why the slopes of each line in control mice were discord should be because of different hematocrit values among mice, as BPA must be distributed to plasma fraction. The average of the y intercepts from five values (between 7.84 and 27.49) was 16.55 (Fig. 5a). The y intercepts in mice samples were higher than those in human blood, because fluorescence may be emitted from heparin. In the preparation of mice samples, heparin is needed to collect the blood without blood-curdling into a tube. In contrast, human blood was collected into tube containing EDTA-2Na and this is not influent in the fluorescent intensities of samples (data not shown). Next, scattered plots were described in BPA treated mouse (Fig. 5b). The left and right graphs are showing that the 0.6 and 0.9 ml of BPA stock (1,600 ppm ^{10}B of BPA) were administrated intraperitoneally, respectively. The y intercepts in the lines of the left graph (Fig. 5b, black and white plots) were 54.11 and 39.69. The values after the subtraction of background value (16.55) were 23.14 and 37.56, respectively; therefore, the BPA concentrations from the lines were 12.26 ppm and 15.61 ppm (divided by each slope value 1.8869 and 2.4069, respectively). In the right graph of Fig. 5b, the values at the y intercept in black and white plots were 95.78 and 153.9 after the subtraction of background value, respectively. Therefore, concentrations in 0.9 ml treated mice were 32.69 ppm and 59.84 ppm, respectively.

We next compared our new method to ICP method in the measurement of blood concentration of ^{10}B in BPA treated mice. As shown in the left graph of Fig. 6, good correlation was observed between fluorescence intensities and ^{10}B concentrations for BPA. In the graph, the y intercept was 56.637, and the value after the subtraction of background
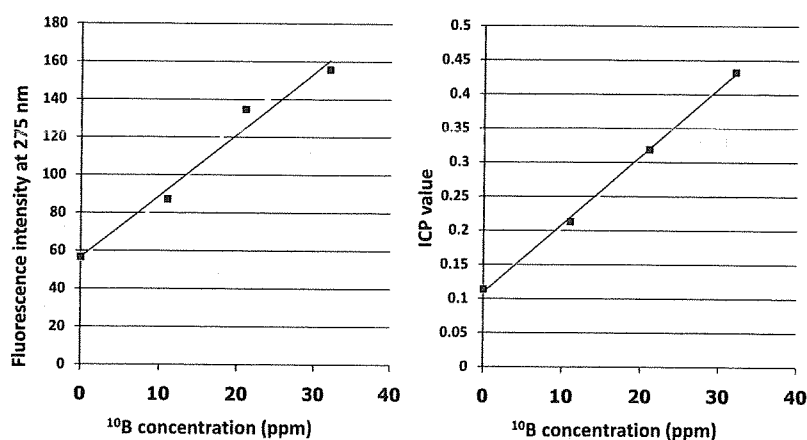

Fig. 6. The comparison of the new method and ICP method in the samples derived from a BPA treated mouse. Left panel is showing the relationship between fluorescence intensity and added BPA concentration. The equations of lines for the scattered plots were y = 3.2477 x + 56.637 (R^2 = 0.9756). Right panel is showing the relationship between the relative values for boron evaluated by ICP and added BPA concentration from the same mouse. The equation of line for the scattered plots was y = 0.01 x + 0.109 (R^2 = 0.9988).

intensity, 16.55 (obtained from Fig. 5a) was 40.087. Therefore, the estimated concentration after divided by 3.2477 (slope value) was 12.34 ppm. As well as the left graph, good correlations were observed between ICP value and ^{10}B concentrations for BPA. In the graph, the y intercept was 0.109. The background value in ICP was almost zero; therefore, estimated concentration after divided by 0.01 (slope value) was 10.9 ppm. It is clearly shown that the difference between the two estimated concentrations in each method is small (12.34 ppm vs 10.9 ppm). There is still difference of 1.44 ppm, but this difference may be mainly brought by the dispersion of background values in mice experiment as shown in Fig. 5a. In the estimation of background fluorescence intensity in mice, we set the average background value, 16.55, from five mice data of Fig. 5a. However, this is not actual background value for each BPA treated mouse. If we could collect the blood to estimate the background level before BPA treatment in the same mouse, more exact BPA concentration should be detected. In the case of a patient, it is possible to collect the blood just before the BPA treatment for a detection of the background level of each patient. Therefore, exact ^{10}B concentrations of BPA can be estimated by our new method in BPA treated patient as well as ICP method.

CONCLUSION

We established a new method to measure only BPA in blood sample by detecting fluorescence based on the characteristics of phenylalanine. This method will be especially useful for BPA measurement in patients undergoing BNCT by concomitant use of BPA and BSH.

ACKNOWLEDGEMENT

REFERENCES

1. Mishima, Y., Honda, C., Ichihashi, M., Obara, H., Hiratsuka, J., Fukuda, H., Karashima, H., Kobayashi, T., Kanda, K. and Yoshino, K. (1989) Treatment of malignant melanoma by single thermal neutron capture therapy with melanoma-seeking 10B-compound. *Lancet* **2**: 388–389.

2. Hatanaka, H. (1991) Boron-Neutron Capture Therapy for tumors, in "Glioma", A. Karim & ER. Laws. Ed. Springer-Verlag, Berlin, New York. 233–270.

3. Kato, I., Ono, K., Sakurai, Y., Ohmae, M., Maruhashi, A., Imahori, Y., Kirihata, M., Nakazawa, M. and Yura, Y. (2004) Effectiveness of BNCT for recurrent head and neck malignancies. *Appl. Radiat. Isot.* **61**: 1069–1073.

4. Aihara, T., Hiratsuka, J., Morita, N., Uno, M., Sakurai, Y., Maruhashi, A., Ono, K. and Harada, T. (2006) First clinical case of boron neutron capture therapy for head and neck malignancies using ^{18}F-BPA PET. *Head Neck.* **28**: 850–852.

5. Suzuki, M., Sakurai, Y., Hagiwara, S., Masunaga, S., Kinashi, Y., Nagata, K., Maruhashi, A., Kudo, M. and Ono, K. (2007) First attempt of boron neutron capture therapy (BNCT) for hepatocellular carcinoma, *Jpn. J. Clin. Oncol.* **37**: 376–381.

6. Ono, K., Masunaga, S., Kinashi, Y., Takagaki, M., Akaboshi, M., Kobayashi, T. and Akuta, K. (1996) Radiobiological evidence suggesting heterogeneous microdistribution of boron compounds in tumors: its relation to quiescent cell population and tumor cure in neutron capture therapy. *Int. J. Radiat. Oncol. Biol. Phys.* **34**: 1081–1086.

7. Ono, K., Masunaga, S., Suzuki, M., Kinashi, Y., Takagaki, M. and Akaboshi, M. (1999) The combined effect of boronophenylalanine and borocaptate in boron neutron capture therapy for SCCVII tumors in mice. *Int. J. Radiat. Oncol. Biol. Phys.* **43**: 431–436.

8. Barth, R. F., Yang, W., Rotaru, J. H., Moeschberger, M. L., Boesel, C. P., Soloway, A. H., Joel, D. D., Nawrocky, M. M. M., Ono, K. and Goodman, J. H. (2000) Boron neutron capture therapy of brain tumors: enhanced survival and cure following blood-brain barrier disruption and intracarotid injection of sodium borocaptate and boronophenylalanine. *Int. J. Radiat. Oncol. Biol. Phys.* **47**: 209–218.

9. Kawabata, S., Miyatake, S., Kuroiwa, T., Yokoyama, K., Doi, A., Iida, K., Miyata, S., Nonoguchi, N., Michiue, H., Takahashi, M., Inomata, T., Imahori, Y., Kirihata, M., Sakurai, Y., Maruhashi, A., Kumada, H. and Ono, K. (2009) Boron neutron capture therapy for newly diagnosed glioblastoma. *J. Radiat. Res.* **50**: 51–60.

10. Miyatake, S., Kawabata, S., Kajimoto, Y., Aoki, A., Yokoyama, K., Yamada, M., Kuroiwa, T., Tsuji, M., Imahori, Y., Kirihata, M., Sakurai, Y., Masunaga, S., Nagata, K., Maruhashi, A. and Ono, K. (2005) Modified boron neutron capture therapy for malignant gliomas performed using epithermal neutron and two boron compounds with different accumulation mechanisms: an efficacy study based on findings on neuroimages. *J. Neurosurg.* **103**: 1000–1009.

11. Takagaki, M., Oda, Y., Miyatake, S., Kikuchi, H., Kobayashi, T., Sakurai, Y., Osawa, M., Mori, K. and Ono, K. (1997) Boron neutron capture therapy: preliminary study of BNCT with sodium borocaptate (Na2B1 2H1 1SH) on glioblastoma. *J Neurooncol.* **35**: 177–185.

12. Munck af Rosenschöld, P. M., Verbakel, W. F., Ceberg, C. P., Stecher-Rasmussen, F. and Persson, B. R. (2001) Toward clinical application of prompt gamma spectroscopy for in vivo monitoring of boron uptake in boron neutron capture therapy. *Med Phys.* **28**: 787–795.

13. Hiratsuka, J., Yoshino, K., Kondoh, H., Imajo, Y. and Mishima, Y. (2000) Biodistribution of boron concentration on melanoma-bearing hamsters after administration of *p*-, *m*-, *o*-boronophenylalanine. *Jpn. J. Cancer Res.* **91**: 446–450.

14. Biochemical Data Book, pp43, Tokyo Kagaku Dojin.

CASE REPORT

Retreatment of recurrent malignant pleural mesothelioma with cisplatin and pemetrexed

Hidetoshi Hayashi · Isamu Okamoto · Yasuko Ichikawa ·
Masaki Miyazaki · Hiroshige Yoshioka · Kei Kunimasa ·
Kazuhiko Nakagawa

Abstract Combination chemotherapy with cisplatin and
pemetrexed is the most active first-line regimen for malig-
nant pleural mesothelioma (MPM). However, no drugs have
been approved for second-line treatment of MPM, with
effective regimens remaining to be identified for patients in
relapse. We have now evaluated the combination of cisplatin
and pemetrexed for retreatment of patients with recurrent
MPM. Four men with MPM, all of whom received initial
treatment with cisplatin and pemetrexed, underwent re-
treatment with this drug combination. Two of the patients
achieved an objective response to the first-line chemotherapy
with no evidence of disease progression for 6.4 or
11.4 months, respectively. The other two patients had stable
disease with a duration of 7.8 or 5.0 months, respectively.
The two patients who showed an objective response to first-
line chemotherapy showed a partial response to retreatment,
with a time to progression of 5.0 or 8.2 months, whereas the
other two patients had progressive disease with a time to
progression of 1.0 or 1.4 months, respectively. Retreatment
with cisplatin plus pemetrexed was generally well tolerated.
Retreatment with cisplatin and pemetrexed is a potential
therapeutic option for certain patients with recurrent epi-
thelioid MPM, possibly including those who show tumor
regression with a time to progression of 6 months or more
after the initial chemotherapy. Further studies are warranted
to evaluate the efficacy of such retreatment and to clarify the
criteria for patient selection.

Introduction

Malignant pleural mesothelioma (MPM) is a highly
aggressive neoplasm. Treatment of MPM patients with the
combination of cisplatin and pemetrexed has been associated
with an increased survival time (12.1 vs. 9.3 months), longer
time to progression (5.7 vs. 3.9 months), and greater
response rate (41.3% vs. 16.7%), as well as with improved
pulmonary function and symptom control compared with
treatment with cisplatin alone [1, 2]. However, most patients
eventually manifest disease progression after the initial
response to such combination chemotherapy. Although a
previous study has suggested that second-line chemotherapy
after initial treatment with cisplatin and pemetrexed has a
positive impact on the survival of MPM patients [3], no drugs
have been approved for second-line treatment of MPM.
Effective chemotherapy is thus needed for the treatment of
patients with MPM who relapse after first-line chemother-
apy. We now present a report of four patients with recurrent
MPM who received an initial course of treatment with
pemetrexed and cisplatin and who subsequently underwent
retreatment with this drug combination.

Case report

Four patients with MPM underwent retreatment with cis-
platin and pemetrexed. Treatment response was evaluated

H. Hayashi · I. Okamoto (✉) · Y. Ichikawa · M. Miyazaki ·
K. Nakagawa
Department of Medical Oncology,
Kinki University School of Medicine,
377-2 Ohno-higashi, Osaka-Sayama, Osaka 589-8511, Japan
e-mail: chi-okamoto@dotd.med.kindai.ac.jp

H. Yoshioka · K. Kunimasa
Department of Respiratory Medicine,
Kurashiki Central Hospital, 1-1-1 Miwa,
Kurashiki, Okayama 710-0047, Japan

🍂 Springer